A cell-centered pressure-correction scheme for the compressible Euler equations

Raphaele Herbin, Jean-Claude Latché, Chady Zaza

A cell-centered pressure-correction scheme for the compressible Euler equations

Raphaèle Herbin *
Aix-Marseille Université, Centrale Marseille, I2M, UMR CNRS 7373, France

Jean-Claude Latché †
Institut de Radioprotection et de Sûreté Nucléaire (IRSN), France

and

Chady Zaza‡
CEA DEN/DANS/DM2S/STMF/LMEC. CEA Cadarache, 13108 St-Paul-lez-Durance, and
Aix-Marseille Université, Centrale Marseille, I2M, UMR CNRS 7373, France

We propose a robust pressure-correction scheme for the numerical solution of the compressible Euler equations discretised by a colocated finite volume method. The scheme is based on an internal energy formulation, which ensures that the internal energy is positive. More generally, the scheme enjoys fundamental stability properties: without restriction on the time step, both the density and the internal energy are positive, the integral of the total energy over the computational domain is preserved thanks to an estimate on the discrete kinetic energy, and a discrete entropy inequality is satisfied. These stability properties ensure the existence of a solution to the scheme. The internal energy balance features a corrective source term which is needed for the scheme to compute the correct shock solutions: we are indeed able to prove a Lax consistency type convergence result, in the sense that, under some compactness assumptions, the limit of a converging sequence of approximate solutions obtained with space and time discretisation steps tending to zero is an entropy weak solution of the Euler equations. Moreover, constant pressure and velocity are preserved through contact discontinuities. The obtained theoretical results and the scheme accuracy are verified by numerical experiments; a numerical stabilisation is introduced in order to reduce the oscillations which appear for some tests. The qualitative behaviour of the scheme is assessed on 1D and 2D Riemann problems and compared with other schemes.

Keywords: Finite-volume methods, compressible flows, pressure-correction methods.

1. Introduction

In this work we address the numerical solution of the compressible Euler equations:

$$\partial_t \rho + \mathrm{div}(\rho \boldsymbol{u}) = 0, \tag{1a}$$

$$\partial_t (\rho \boldsymbol{u}) + \mathbf{div}(\rho \boldsymbol{u} \otimes \boldsymbol{u}) + \boldsymbol{\nabla} p = 0, \tag{1b}$$

$$\partial_t (\rho E) + \mathrm{div}(\rho E \boldsymbol{u}) + \mathrm{div}(p \boldsymbol{u}) = 0, \tag{1c}$$

$$\rho \geqslant 0,\ e \geqslant 0,\ p = \wp(\rho, e),\ E = \frac{1}{2}|\boldsymbol{u}|^2 + e, \tag{1d}$$

where $\boldsymbol{u}$, ρ, p, E and e denote the velocity, the density, the pressure, the total energy and the internal energy respectively. The function $\wp$ is the equation of state for an ideal gas, which we extend by 0 for negative ρ and e, for the sole purpose of the mathematical study of the scheme:

$$\wp(\rho, e) = \begin{cases} (\gamma - 1)\rho e \text{ if } \rho \geqslant 0 \text{ and } e \geqslant 0, \\ 0 \text{ otherwise.} \end{cases} \tag{2}$$

*Corresponding author. Email: raphaele.herbin@univ-amu.fr
†Email: jean-claude.latche@irsn.fr
‡Email: chady.zaza@free.fr

The problem is defined over $\Omega \times (0,T)$, where Ω is an open polygonal bounded connected subset of $\mathbb{R}^d$, $d = 1$, 2 or 3 and $(0,T)$ is a finite time interval. The system is complemented by initial conditions for ρ, e and $\boldsymbol{u}$, which are denoted by ρ_0, e_0 and $\boldsymbol{u}_0$, with $\rho_0 > 0$ and $e_0 > 0$. In the presentation and in the study of the numerical scheme, we shall consider for simplicity the boundary condition $\boldsymbol{u} \cdot \boldsymbol{n} = 0$, where $\boldsymbol{n}$ stands for the outward normal vector to the boundary, but other conditions are also easily implemented (see Section 5).

The scheme proposed in this paper falls in the class of pressure correction methods. Such schemes were originally introduced by [2] and [40] for the incompressible Navier-Stokes equations, see also [16] for a review of most of the variants. They were adapted to compressible flows in the pioneering works by [17, 18] in an attempt to avoid the stringent stability conditions such as a CFL condition based on the celerity of the fastest waves; these latter algorithms may be seen as an extension to the compressible case of the celebrated MAC scheme, introduced some years before by [19]. Numerous projection schemes followed; many of them used staggered finite volume space discretisations, we refer to the references in [15]; others were on colocated grids as the ones we choose here, see [22, 37, 7, 26, 38, 24, 4, 30, 32, 41, 23, 25, 34, 35, 33, 39, 1, 43, 5]. Algorithms proposed in these works may be essentially implicit-in-time, and the pressure correction step is then an ingredient of a SIMPLE-like iterative procedure such as [36]; conversely, several of these schemes propose a single (or a limited number of) prediction and correction step(s), as in the previously mentioned projection methods for incompressible flows.

The semi-implicit fractional step scheme proposed in the present paper belongs to this latter category, since only one correction step is implemented. The unknowns associated to the velocity and the scalar variables are colocated at the center of the meshes. Developed in the spirit of the recent schemes based on staggered meshes [20, 21, 15], the proposed algorithm enjoys the following salient features:

First, upwinding is performed equation per equation with respect to the material velocity only. This approximation of the mass balance ensures the positivity of the density.

Second, a discretisation of an internal energy balance equation is used rather than of the total energy balance, which allows to preserve the positivity of the internal energy by standard upwinding techniques. It is however well known that computing the solution with the internal energy rather than the total energy yields wrong shock speeds (see e.g.[42]). A correction term is added to the discrete internal energy balance to obtain the correct shock speeds; it is computed as follows. First, a discrete kinetic energy equation is established from the discrete momentum and mass balances; this equation features a positive residual term. It may be anticipated that for regular solutions, this term tends to zero when the space and time steps tend to zero; but for shock solutions, it subsists as a measure borne by the shocks. The idea is thus to add the opposite of this residual term in the internal energy balance equation. For colocated discretisations, summing the kinetic and internal energy balance yields *in fine* some kind of conservative discrete total energy balance; weak consistency of the total energy is thus ensured, which implies that correct shock speeds are obtained. Note that the situation is simpler here than for staggered discretisations: in this latter case, the discrete kinetic and internal energy balance are not associated to the same mesh [20, 21, 15]. Here as in these latter works, the energy of the flow, *i.e.* the integral of the total energy over the computational domain is preserved; since the density and internal energy remain positive, this total energy preservation yields an unconditional stability property.

In addition, the pressure correction step couples the mass and internal energy balance equations, with two beneficial consequences: first, we recover the structure which allows to establish an entropy inequality; second, with the specific considered equation of state (and, more generally, for all equations of state such that the product ρe is a function of the pressure only), the scheme keeps the velocity and pressure constant across 1D contact discontinuities.

Finally, a stabilisation is obtained from the above-mentioned upwinding of the convection terms with respect to the material velocity only, possibly combined with a nonlinear viscosity [27] when needed. Consequently, the scheme does not blow up when the celerity of waves tends to infinity or, in other words, when the Mach number tends to zero.

This article is organised as follows. In Section 2, a cell-centered finite-volume discretisation of the compressible Euler equations is introduced along with the pressure-correction scheme. Section 3 is devoted to the positivity of the density and energy and to the stability of the scheme. A proof of existence of a discrete solution in the multi-dimensional case is also given. In Section 4, the scheme is proven to be consistent in the Lax sense, *i.e.* a limit of a converging sequence of solutions to the scheme obtained with mesh and time steps tending to 0 is shown to satisfy the weak form of the Euler equations (1). Numerical experiments are performed in Section 5; the scheme is also compared to an alternative already existing pressure correction scheme [31], which is described in the appendix.

2. Space and time discretisation

2.1 *Finite volume mesh of Ω and discrete space unknowns*

Let $\mathcal{M}$ be a family of disjoint convex polygonal subsets of Ω, called *control volumes*, such that $\bar{\Omega} = \cup_{K\in\mathcal{M}} \bar{K}$. The d-dimensional measure (area if $d = 2$, volume if $d = 3$) of a control volume K is denoted by $|K|$, its boundary and the $(d-1)$-dimensional measure of its boundary by $\partial K = \bar{K} \setminus K$ and $|\partial K|$. The edges ($d = 2$) or faces ($d = 3$) of all control volumes of $\mathcal{M}$ are included in hyperplanes of the space $\mathbb{R}^d$; for short, they will be referred to as faces in the rest of the paper, whatever the space dimension. The $(d-1)$-dimensional measure of a face $\sigma \in \mathcal{E}$ is denoted $|\sigma|$. We define $\mathcal{E}$, $\mathcal{E}_{\rm int}$, $\mathcal{E}_{\rm ext}$ and $\mathcal{E}(K)$ as the set of faces of the mesh, the subset of internal faces, of faces lying on the domain boundary and of faces of the cell K respectively. Given two neighbouring control volumes $K, L \in \mathcal{M}^2$, we denote their common face $\sigma = K|L$. The normal vector to a face σ pointing outwards the control volume K is denoted by $\boldsymbol{n}_{K,\sigma}$. Note that

$$\sum_{\sigma\in\mathcal{E}(K)} |\sigma|\ \boldsymbol{n}_{K,\sigma} = 0. \tag{3}$$

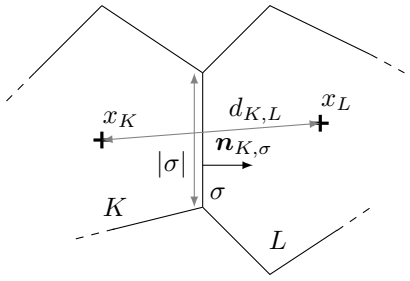

FIG. 1. Cell-centered finite-volume discretisation.

Let $\mathcal{P} = (\boldsymbol{x}_K)_{K\in\mathcal{M}}$ be a family of points of Ω with, for $K \in \mathcal{M}$, $\boldsymbol{x}_K \in K$. For a face $\sigma \in \mathcal{E}_{\rm int}$ separating the cells K and L, the point $\boldsymbol{x}_\sigma$ is defined as the intersection between the segment $[\boldsymbol{x}_K \boldsymbol{x}_L]$ and the hyperplane containing σ.

The discretisation is colocated in the sense that the discrete unknowns are associated to the same location. The discrete unknowns are thus $(\boldsymbol{u}_K)_{K\in\mathcal{M}}$ for the velocity, $(\rho_K)_{K\in\mathcal{M}}$, $(p_K)_{K\in\mathcal{M}}$ and $(e_K)_{K\in\mathcal{M}}$ for the density, pressure and internal energy respectively.

2.2 *Discrete gradient and divergence*

The discrete velocity divergence and pressure gradient operators are defined by duality. Indeed, we look for a discrete equivalent of the classical *div-grad duality property*: if $\boldsymbol{u} : \Omega \to \mathbb{R}^d$ and $p : \Omega \to \mathbb{R}$ are sufficiently regular functions such that $\boldsymbol{u} \cdot \boldsymbol{n} = 0$ on $\partial\Omega$ then:

$$\int_\Omega (p \operatorname{div} \boldsymbol{u} + \boldsymbol{u} \cdot \boldsymbol{\nabla} p)\ \mathrm{d}\boldsymbol{x} = 0.$$

Definition 2.1 (Discrete divergence and discrete gradient) *Let K, $L \in \mathcal{M}$ be two neighbouring cells, separated by the face σ. We set*

$$\mathrm{d}_{K,L} = |\boldsymbol{x}_K - \boldsymbol{x}_L| \text{ and } \mathrm{d}_{K,\sigma} = |\boldsymbol{x}_K - \boldsymbol{x}_\sigma|, \tag{4a}$$

$$\alpha_{K,\sigma} = \frac{d_{L,\sigma}}{d_{K,L}} \text{ and } \alpha_{L,\sigma} = \frac{d_{K,\sigma}}{d_{K,L}}, \tag{4b}$$

where $|\cdot|$ stands for the Euclidean norm in $\mathbb{R}^d$. Let $(\boldsymbol{u}_K)_{K\in\mathcal{M}}$ be a given discrete velocity; its discrete divergence is defined by:

$$\mathrm{div}_K\, \boldsymbol{u} = \frac{1}{|K|} \sum_{\sigma\in\mathcal{E}(K)} |\sigma|\; u_{K,\sigma}, \quad \forall K \in \mathcal{M}, \tag{5}$$

where

$$u_{K,\sigma} = \begin{cases} \boldsymbol{u}_\sigma \cdot \boldsymbol{n}_{K,\sigma} = (\alpha_{K,\sigma}\boldsymbol{u}_K + \alpha_{L,\sigma}\boldsymbol{u}_L)\cdot \boldsymbol{n}_{K,\sigma} & \text{for } \sigma = K|L \in \mathcal{E}_{\mathrm{int}}, \\ 0 & \text{for } \sigma \in \mathcal{E}_{\mathrm{ext}}. \end{cases} \tag{6}$$

Despite the interpolation formula (6)*, the divergence operator is generally not consistent (i.e. the discrete and continuous divergence operators do not coincide for affine velocity fields) except when the point $\boldsymbol{x}_\sigma$ is the mass center of σ; this is the case for instance for rectangles and simplices in two space dimensions (of course, with a specific choice for $\boldsymbol{x}_K$, namely if $\boldsymbol{x}_K$ is chosen as the mass center of K for rectangles and the circumcenter of K for simplices) and for rectangular parallelepipeds in three space dimensions (with $\boldsymbol{x}_K$ the mass center of K). Next we define the discrete gradient of a pressure field $(\boldsymbol{u}_K)_{K\in\mathcal{M}}$ by*

$$\boldsymbol{\nabla}_K\, p = \frac{1}{|K|}\Big[\sum_{\sigma=K|L} |\sigma|\; (\alpha_{L,\sigma}p_K + \alpha_{K,\sigma}p_L)\; \boldsymbol{n}_{K,\sigma} + \sum_{\sigma\in\mathcal{E}_{\mathrm{ext}}\cap\mathcal{E}(K)} |\sigma|\; p_K\, \boldsymbol{n}_{K,\sigma}\Big], \tag{7}$$

for all $K \in \mathcal{M}$, where the notation $\sum_{\sigma=K|L}$ means that the sum is over the neighbouring cells L of K, and that σ stands for the common face $K|L$ of K and L.

Lemma 2.2 *Under the assumptions of Definition 2.1, the discrete divergence and gradient operators satisfy:*

$$\nabla_K p = \frac{1}{|K|} \sum_{\sigma=K|L} |\sigma|\, \alpha_{K,\sigma}\, (p_L - p_K)\; \boldsymbol{n}_{K,\sigma}, \tag{8}$$

$$\sum_{K\in\mathcal{M}} |K|\, (\boldsymbol{u}_K \cdot \boldsymbol{\nabla}_K\, p + p_K\, \mathrm{div}_K\, \boldsymbol{u}) = 0. \tag{9}$$

Furthermore,

$$\begin{aligned} &\boldsymbol{u}_K \cdot \boldsymbol{\nabla}_K\, p + p_K\, \mathrm{div}_K\, \boldsymbol{u} = \mathrm{div}_K(p\boldsymbol{u}) = \frac{1}{|K|} \sum_{\sigma\in\mathcal{E}(K)} |\sigma|\, (p\boldsymbol{u})_\sigma \cdot \boldsymbol{n}_{K,\sigma} \\ &\text{with } (p\boldsymbol{u})_\sigma = \begin{cases} \alpha_{K,\sigma}p_L\boldsymbol{u}_K + \alpha_{L,\sigma}p_K\boldsymbol{u}_L \text{ for } \sigma = K|L \in \mathcal{E}_{\mathrm{int}}, \\ 0 \text{ if } \sigma \in \mathcal{E}_{\mathrm{ext}}. \end{cases} \end{aligned} \tag{10}$$

Proof 1 *The equality* (8) *is a direct consequence of* (3) *and the fact that $\alpha_{K,\sigma} + \alpha_{L,\sigma} = 1$. From the definition of the discrete divergence operator given by Equation* (5)*, we have*

$$\sum_{K\in\mathcal{M}} |K|\, p_K\, \mathrm{div}_K\, \boldsymbol{u} = \sum_{K\in\mathcal{M}} p_K \sum_{\sigma=K|L} |\sigma|\; \alpha_{K,\sigma}\; \boldsymbol{u}_K\cdot\boldsymbol{n}_{K,\sigma} + \sum_{K\in\mathcal{M}} p_K \sum_{\sigma=K|L} |\sigma|\; \alpha_{L,\sigma}\, \boldsymbol{u}_L\cdot\boldsymbol{n}_{K,\sigma}.$$

Reordering the second sum of the right hand side as:

$$\sum_{K\in\mathcal{M}} p_K \sum_{\sigma=K|L} |\sigma|\ \alpha_{L,\sigma}\,\boldsymbol{u}_L\cdot\boldsymbol{n}_{K,\sigma} = \sum_{\substack{\sigma\in\mathcal{E}_{\rm int}\\ \sigma=K|L}} |\sigma|\ \left(\alpha_{L,\sigma}\,p_K\,\boldsymbol{u}_L\cdot\boldsymbol{n}_{K,\sigma} + \alpha_{K,\sigma}\,p_L\,\boldsymbol{u}_K\cdot\boldsymbol{n}_{L,\sigma}\right)$$
$$= \sum_{K\in\mathcal{M}} \sum_{\sigma=K|L} |\sigma|\ \alpha_{K,\sigma}\,p_L\,\boldsymbol{u}_K\cdot\boldsymbol{n}_{L,\sigma},$$

we get

$$\sum_{K\in\mathcal{M}} |K|\ p_K\ \mathrm{div}_K\,\boldsymbol{u} = \sum_{K\in\mathcal{M}} \boldsymbol{u}_K\cdot\sum_{\sigma=K|L} |\sigma|\ \alpha_{K,\sigma}\ (p_K-p_L)\ \boldsymbol{n}_{K,\sigma},$$

which, thanks to (8)*, concludes the proof of* (9)*. Let us now turn to the proof of* (10)*. By definition of the discrete operators, using once again* (8)*, we get:*

$$|K|\ (\boldsymbol{u}_K\cdot\boldsymbol{\nabla}_K\,p + p_K\,\mathrm{div}_K\,\boldsymbol{u}) = \sum_{\sigma=K|L} |\sigma|\ \Big[\alpha_{K,\sigma}\,(p_L-p_K)\,\boldsymbol{u}_K + p_K\,(\alpha_{K,\sigma}\boldsymbol{u}_K+\alpha_{L,\sigma})\,\boldsymbol{u}_L\Big]\cdot\boldsymbol{n}_{K,\sigma}$$
$$= \sum_{\sigma=K|L} |\sigma|\ \Big[\alpha_{K,\sigma}\,p_L\boldsymbol{u}_K + \alpha_{L,\sigma}\,p_K\boldsymbol{u}_L\Big]\cdot\boldsymbol{n}_{K,\sigma}$$

which concludes the proof.

2.3 *Upwind choice and discrete convection operators*

The terms $\mathrm{div}(\rho\boldsymbol{u})$ in the mass balance equation (1a) and $\mathrm{div}(\rho e\boldsymbol{u})$ in the momentum balance equation (1b) are discretised as follows. The numerical mass flux across a face σ is thus chosen as:

$$F_{K,\sigma} = |\sigma|\ \rho_\sigma u_{K,\sigma}, \tag{11}$$

where $u_{K,\sigma}$ is defined by (6) and ρ_σ the upwind value of ρ on σ. We recall that, for a given discrete scalar field $(a_K)_{K\in\mathcal{M}}$, the upwind choice a_σ on a face $\sigma=K|L\in\mathcal{E}_{\rm int}$ with respect to $u_{K,\sigma}$ is defined by:

$$a_\sigma = \begin{cases} a_K \text{ if } u_{K,\sigma}>0,\\ a_L \text{ otherwise.}\end{cases} \tag{12}$$

We may thus define a discrete divergence operator of the functions $\rho\boldsymbol{u}$ and $\rho e\boldsymbol{u}$ as:

$$\mathrm{div}_K(\rho\boldsymbol{u}) = \frac{1}{|K|}\sum_{\sigma\in\mathcal{E}(K)} F_{K,\sigma} \text{ and } \mathrm{div}_K(\rho e\boldsymbol{u}) = \frac{1}{|K|}\sum_{\sigma\in\mathcal{E}(K)} e_\sigma F_{K,\sigma}, \tag{13}$$

where e_σ is the upwind value of e at the face σ with respect to $F_{K,\sigma}$.

The non linear convection term $\mathbf{div}(\rho\boldsymbol{u}\otimes\boldsymbol{u})$ in equation (1b) is discretised as

$$\mathbf{div}_K(\rho\boldsymbol{u}\otimes\boldsymbol{v}) = \frac{1}{|K|}\sum_{\sigma\in\mathcal{E}(K)} F_{K,\sigma}\ \boldsymbol{v}_{\sigma,cv}, \tag{14}$$

where $\boldsymbol{v}_{\sigma,cv}$ is defined componentwise as either the upwind face value of $\boldsymbol{v}$ ($\delta^{\rm up}=1$) with respect to $F_{K,\sigma}$ or its centered value ($\delta^{\rm up}=0$):

$$\boldsymbol{v}_{\sigma,cv} = \varepsilon_{K,\sigma}\,\boldsymbol{v}_K + (1-\varepsilon_{K,\sigma})\,\boldsymbol{v}_L \quad \text{with } \varepsilon_{K,\sigma} = \begin{cases} (1+\delta^{\rm up})/2 \text{ if } F_{K,\sigma}>0,\\ (1-\delta^{\rm up})/2 \text{ otherwise.}\end{cases} \tag{15}$$

All the theoretical results presented hereafter apply for $\delta^{\rm up}=0$ and $\delta^{\rm up}=1$.

2.4 *Time discretisation*

For the sake of clarity, we start with an implicit-in-time scheme. Let δt be a time discretisation step, which is assumed to be constant. Let $N \in \mathbb{N}$ be the number of time discretisation steps and $\delta t = T/N$ the time step. The discrete time is defined as $t_n = n\delta t$ for $n \in [\![0, N]\!]$. The discrete unknowns are the discrete density, internal energy and velocity fields $\{\rho_K^n, e_K^n, \boldsymbol{u}_K^n; K \in \mathcal{M},\ n \in [\![1, N]\!]\}$. Assuming a given initial state $(\rho_K^0, \boldsymbol{u}_K^0, e_K^0)_{K\in\mathcal{M}}$ and $p_K^0 = (\gamma-1)\rho_K^0 e_K^0$, the implicit-in-time discretisation of Problem (1) reads:

$$\forall K \in \mathcal{M},\ \forall n \in [\![0, N-1]\!],$$

$$\frac{1}{\delta t}(\rho_K^{n+1} - \rho_K^n) + \mathrm{div}_K(\rho^{n+1}\boldsymbol{u}^{n+1}) = 0, \tag{16a}$$

$$\frac{1}{\delta t}(\rho_K^{n+1}\boldsymbol{u}_K^{n+1} - \rho_K^n\boldsymbol{u}_K^n) + \mathbf{div}_K(\rho^{n+1}\boldsymbol{u}^{n+1}\otimes\boldsymbol{u}^{n+1}) + \boldsymbol{\nabla}_K\, p^{n+1} = 0, \tag{16b}$$

$$\frac{1}{\delta t}(\rho_K^{n+1}e_K^{n+1} - \rho_K^n e_K^n) + \mathrm{div}_K(\rho^{n+1}e^{n+1}\boldsymbol{u}^{n+1}) + p_K^{n+1}\,\mathrm{div}_K\,\boldsymbol{u}^{n+1} = S_K^{n+1}, \tag{16c}$$

$$p_K^{n+1} = (\gamma-1)\ \rho_K^{n+1}\ e_K^{n+1}, \tag{16d}$$

where div_K is the discrete divergence operator defined by (5) and (13), $\mathbf{div}_K$ stands for its vector-valued extension defined by (14), and $\boldsymbol{\nabla}_K$ is the discrete gradient operator defined by (7). Note that, as announced in the introduction, a balance equation for the internal energy (Equation (16c)) is used instead of a total energy balance, with a corrective term S_K^{n+1} at the right hand side needed for consistency. For the implicit scheme, this term reads

$$S_K^{n+1} = \frac{1}{2\delta t}\,\rho_K^n\,|\boldsymbol{u}_K^{n+1} - \boldsymbol{u}_K^n|^2 + \frac{\delta^{\mathrm{up}}}{4|K|}\sum_{\sigma=K|L}\left|\boldsymbol{u}_K^{n+1} - \boldsymbol{u}_L^{n+1}\right|^2(|F_{K,\sigma}^{n+1}| - F_{K,\sigma}^{n+1}).$$

It is built so as to compensate the numerical dissipation term appearing in the derivation of the kinetic energy balance, as detailed in Section 3. As shown in the sequel, the positivity of the term S_K^{n+1} is a sufficient condition for the positivity of the internal energy.

In real-life applications, the implicit scheme is expensive in terms of memory and CPU requirements so that semi-implicit schemes are generally preferred. We choose here a class of pressure-correction schemes recently developed for staggered finite volumes in [21]. In the same spirit as projection schemes for the incompressible Navier-Stokes equations, a tentative velocity is computed using the momentum balance (18), with a scaling of the pressure introduced so as to recover a discrete kinetic inequality, see Remark 3.6. Then a non-linear problem is solved in order to update the pressure, internal energy and density and correct the velocity (Equation (20a) below) such that the mass balance (20b) and the internal energy balance (20c) are verified.

Initialization: for $K \in \mathcal{M}$,

$$\rho_K^{-1} = \frac{1}{|K|}\int_K \rho_0\ \mathrm{d}\boldsymbol{x},\ \boldsymbol{u}_K^0 = \frac{1}{|K|}\int_K \boldsymbol{u}_0\ \mathrm{d}\boldsymbol{x},\ e_K^0 = \frac{1}{|K|}\int_K e_0\ \mathrm{d}\boldsymbol{x}, \tag{17a}$$

$$\frac{1}{\delta t}(\rho_K^0 - \rho_K^{-1}) + \delta t\,\mathrm{div}_K(\rho^0\boldsymbol{u}^0) = 0, \tag{17b}$$

$$p_K^0 = (\gamma-1)\ \rho_K^0\, e_K^0. \tag{17c}$$

Iterations: for $n \in [\![0, N-1]\!]$,

- **Prediction**: compute $\tilde{\boldsymbol{u}}_K^{n+1}$ by solving for all $K \in \mathcal{M}$,

$$\frac{1}{\delta t}(\rho_K^n\tilde{\boldsymbol{u}}_K^{n+1} - \rho_K^{n-1}\boldsymbol{u}_K^n) + \mathbf{div}_K(\rho^n\boldsymbol{u}^n\otimes\tilde{\boldsymbol{u}}^{n+1}) + \widetilde{\boldsymbol{\nabla}_K\, p^n} = 0, \tag{18}$$

$$\text{with } \widetilde{\boldsymbol{\nabla}_K\, p^n} = \sqrt{\frac{\rho_K^n}{\rho_K^{n-1}}}\,\boldsymbol{\nabla}_K\, p^n. \tag{19}$$

- **Correction**: compute $\boldsymbol{u}_K^{n+1}$, p_K^{n+1}, e_K^{n+1} and ρ_K^{n+1} by solving the non-linear system of equations obtained by writing, for all $K \in \mathcal{M}$,

$$\frac{1}{\delta t}\rho_K^n \left(\boldsymbol{u}_K^{n+1} - \tilde{\boldsymbol{u}}_K^{n+1}\right) + \left(\boldsymbol{\nabla}_K p^{n+1} - \widetilde{\boldsymbol{\nabla}_K p^n}\right) = 0, \tag{20a}$$

$$\frac{1}{\delta t}(\rho_K^{n+1} - \rho_K^n) + \mathrm{div}_K(\rho^{n+1}\boldsymbol{u}^{n+1}) = 0, \tag{20b}$$

$$\frac{1}{\delta t}(\rho_K^{n+1}e_K^{n+1} - \rho_K^n e_K^n) + \mathrm{div}_K(\rho^{n+1}e^{n+1}\boldsymbol{u}^{n+1}) + p_K^{n+1}\,\mathrm{div}_K\,\boldsymbol{u}^{n+1} = S_K^{n+1}, \tag{20c}$$

$$p_K^{n+1} = (\gamma-1)\rho_K^{n+1}e_K^{n+1}. \tag{20d}$$

The proof of the discrete kinetic inequality in Proposition 3.3 below relies on a compatibility condition between the mass balance and the time derivative and convection terms in the momentum balance equation (18) [21]; this condition may be formulated as the fact that the sum of these two terms vanishes for constant velocity fields. Since the mass balance solution is part of the correction step, it is only satisfied at time t_{n-1} when dealing with the momentum balance at time t_n; hence the backward shift in time on the density and the advective mass flux in the momentum balance and the definition of ρ_K^{-1}. For the same reason, the face value $\tilde{\boldsymbol{u}}_\sigma^{n+1}$ in the divergence operator in (18) is constructed according to (15) using $F_{K,\sigma}^n$ as advecting mass flux, while the advected quantities ρ_σ^{n+1} and e_σ^{n+1} in the divergence terms of the discrete mass balance (20b) and internal energy equation (20c) use $F_{K,\sigma}^{n+1}$. Again for stability reasons, these two latter equations need to be coupled, see [34, 35], [15, Section 4] and Section 3 below; this is the reason why both mass balance and energy balance are included in the correction step. The corrective term S_K^{n+1} for the semi-implicit scheme reads:

$$S_K^{n+1} = \frac{1}{2\delta t}\rho_K^{n-1}\left|\tilde{\boldsymbol{u}}_K^{n+1} - \boldsymbol{u}_K^n\right|^2 + \frac{\delta^{\mathrm{up}}}{4|K|}\sum_{\sigma=K|L}\left|\tilde{\boldsymbol{u}}_K^{n+1} - \tilde{\boldsymbol{u}}_L^{n+1}\right|^2 (|F_{K,\sigma}^n| - F_{K,\sigma}^n). \tag{21}$$

As in the case of the implicit scheme, it is built so as to compensate the numerical dissipation terms appearing in the derivation of the kinetic energy balance (see Section 3).

3. Stability of the scheme and existence of a solution

Let us first recall a result on the transport operator [14] which is used to prove the positivity of the approximate density and internal energy. Here and in the sequel, for $a \in \mathbb{R}$, we set $a^+ = \max(a,0)$ and $a^- = -\min(a,0)$. Therefore $|a| = a^+ + a^-$ and $2a^- = |a| - a$.

Lemma 3.1 (see [14, Lemma 2.2]) *Let $(\rho_K)_{K\in\mathcal{M}} \subset \mathbb{R}_+$, $(\rho_K^*)_{K\in\mathcal{M}} \subset \mathbb{R}_+$ and $(u_{K,\sigma})_{\sigma\in\mathcal{E}(K),K\in\mathcal{M}} \subset \mathbb{R}$ be three families of real numbers satisfying:*

$$\forall K \in \mathcal{M},\ \frac{1}{\delta t}(\rho_K - \rho_K^*) + \mathrm{div}_K(\rho\boldsymbol{u}) = 0.$$

Let us assume that, for any internal face $\sigma = K|L$, $u_{K,\sigma} = -u_{L,\sigma}$ and that, for any external face $\sigma \in \mathcal{E}(K)$, $u_{K,\sigma} = 0$. Then, for any families $(y_K)_{K\in\mathcal{M}} \subset \mathbb{R}$ and $(y_K^*)_{K\in\mathcal{M}} \subset \mathbb{R}$, we have:

$$-\sum_{K\in\mathcal{M}}|K|\,(y_K)^-\Big[\frac{1}{\delta t}(\rho_K y_K - \rho_K^* y_K^*) + \mathrm{div}_K(\rho y\boldsymbol{u})\Big] \geqslant \frac{1}{2}\sum_{K\in\mathcal{M}}\frac{|K|}{\delta t}\Big[\rho_K[(y_K)^-]^2 - \rho_K^*[(y_K^*)^-]^2\Big].$$

Proposition 3.2 (Positivity) *Let $n \in [\![0, N-1]\!]$. Assume that $e_K^n \geqslant 0$, $S_K^{n+1} \geqslant 0$ and $\rho_K^n > 0$ for any $K \in \mathcal{M}$, and let ρ_K^{n+1} and e_K^{n+1} satisfy the correction step (20). Then*

$$\forall K \in \mathcal{M},\ \rho_K^{n+1} > 0 \text{ and } e_K^{n+1} \geqslant 0.$$

Proof 2 *The positivity of the density is a consequence of the upwind discretisation of the mass balance equation (20b), see for instance [14, Lemma 2.1]. Let us then show that the internal*

energy remains non-negative as long as the corrective term S_K^{n+1} of the internal energy balance is non-negative. Multiplying the internal energy equation (20c) by $-|K|\ (e_K^{n+1})^-$ and summing over $K \in \mathcal{M}$, we get:

$$
\begin{aligned}
&T_1 + T_2 + T_3 = 0, \ \textit{where}\\
&T_1 = -\sum_{K\in\mathcal{M}} |K|\ (e_K^{n+1})^- \Big[\frac{1}{\delta t}(\rho_K^{n+1} e_K^{n+1} - \rho_K^n e_K^n) + \operatorname{div}_K(e^{n+1}\rho^{n+1}\boldsymbol{u}^{n+1})\Big],\\
&T_2 = -\sum_{K\in\mathcal{M}} |K|\ p_K^{n+1}(e_K^{n+1})^- \operatorname{div}_K(\boldsymbol{u}^{n+1}),\\
&T_3 = \sum_{K\in\mathcal{M}} |K|\ (e_K^{n+1})^- S_K^{n+1}.
\end{aligned}
$$

The term T_2 is equal to zero, thanks to the form of the equation of state (2) *and to the fact that $(e_K^{n+1})^- = -\min(0, e_K^{n+1})$. Since $S_K^{n+1} \geqslant 0$, we have $T_3 \geqslant 0$. Applying Lemma 3.1 on T_1 we get:*

$$
T_1 \geqslant \frac{1}{2}\sum_{K\in\mathcal{M}} \frac{|K|}{\delta t}\Big[\rho_K^{n+1}[(e_K^{n+1})^-]^2 - \rho_K^n[(e_K^n)^-]^2\Big] = \frac{1}{2}\sum_{K\in\mathcal{M}} \frac{|K|}{\delta t}\rho_K^{n+1}\big[(e_K^{n+1})^-\big]^2,
$$

thanks to the fact that $e_K^n \geqslant 0$. Gathering all terms yields

$$
\sum_{K\in\mathcal{M}} \frac{|K|}{\delta t}\rho_K^{n+1}[(e_K^{n+1})^-]^2 \leqslant 0.
$$

As a result, for all $K \in \mathcal{M}$, $\min(e_K^{n+1}, 0) = 0$ and therefore $e_K^{n+1} \geqslant 0$.

Proposition 3.3 (Discrete kinetic energy balance) *Let $(\rho_K^n,\ e_K^n, \boldsymbol{u}_K^n, \tilde{\boldsymbol{u}}_K^n, p_K^n)_{K\in\mathcal{M},\ n\in[\![0,N]\!]}$ be a solution to* (18)-(20)*. Then the following local discrete kinetic energy balance equation holds for all $K \in \mathcal{M}$, $n \in [\![0, N-1]\!]$:*

$$
\frac{1}{2\delta t}\big(\rho_K^n\,|\boldsymbol{u}_K^{n+1}|^2 - \rho_K^{n-1}\,|\boldsymbol{u}_K^n|^2\big) + \frac{1}{2\,|K|}\sum_{\sigma=K|L} \tilde{\boldsymbol{u}}_{\sigma,K}^{n+1}\cdot\tilde{\boldsymbol{u}}_{\sigma,L}^{n+1} F_{K,\sigma}^n + \boldsymbol{u}_K^{n+1}\cdot\boldsymbol{\nabla}_K\, p^{n+1} = R_K^{n+1} - P_K^{n+1},
\tag{22}
$$

with

$$
\begin{aligned}
&\tilde{\boldsymbol{u}}_{\sigma,K} = \tilde{\boldsymbol{u}}_K, \tilde{\boldsymbol{u}}_{\sigma,L} = \tilde{\boldsymbol{u}}_L \ \textit{in the centered case } (\delta^{\mathrm{up}} = 0),\\
&\tilde{\boldsymbol{u}}_{\sigma,K} = \tilde{\boldsymbol{u}}_{\sigma,L} = \tilde{\boldsymbol{u}}_{\sigma,cv} \ \textit{in the upwind case } (\delta^{\mathrm{up}} = 1).
\end{aligned}
\tag{23}
$$

and

$$
R_K^{n+1} = -\frac{1}{2\delta t}\rho_K^{n-1}\big|\tilde{\boldsymbol{u}}_K^{n+1} - \boldsymbol{u}_K^n\big|^2 - \frac{\delta^{\mathrm{up}}}{2\,|K|}\sum_{\sigma=K|L}\big|\tilde{\boldsymbol{u}}_L^{n+1} - \tilde{\boldsymbol{u}}_K^{n+1}\big|^2\left(F_{K,\sigma}^n\right)^-,
\tag{24}
$$

$$
P_K^{n+1} = \frac{\delta t}{2\rho_K^n}\big|\boldsymbol{\nabla}_K\, p^{n+1}\big|^2 - \frac{\delta t}{2\rho_K^{n-1}}\big|\boldsymbol{\nabla}_K\, p^n\big|^2.
\tag{25}
$$

Proof 3 *As in [21], the proof mimicks the continuous case: we multiply the momentum balance by the velocity and use the mass balance twice. The mass balance* (20b) *written at time t_{n-1} reads*

$$
\frac{1}{\delta t}\big(\rho_K^n - \rho_K^{n-1}\big) + \frac{1}{|K|}\sum_{\sigma=K|L} F_{K,\sigma}^n = 0.
\tag{26}
$$

Multiplying this relation by $\tilde{\boldsymbol{u}}_K^{n+1}$ and subtracting from the momentum balance (18) *yields:*

$$
\frac{1}{\delta t}\rho_K^{n-1}\big(\tilde{\boldsymbol{u}}_K^{n+1} - \boldsymbol{u}_K^n\big) + \frac{1}{|K|}\sum_{\sigma=K|L}\big(\tilde{\boldsymbol{u}}_{\sigma,cv}^{n+1} - \tilde{\boldsymbol{u}}_K^{n+1}\big)\ F_{K,\sigma}^n + \widetilde{\boldsymbol{\nabla}_K\, p^n} = 0.
$$

Multiplying by $\frac{1}{2}\tilde{\boldsymbol{u}}_K^{n+1}$ *and using the identity* $2(a-b)a = a^2 - b^2 + (a-b)^2$*, we have:*

$$\frac{1}{2\delta t}\rho_K^{n-1}\Big(\big|\tilde{\boldsymbol{u}}_K^{n+1}\big|^2 - \big|\boldsymbol{u}_K^n\big|^2\Big) + \frac{1}{2\delta t}\rho_K^{n-1}\big|\tilde{\boldsymbol{u}}_K^{n+1} - \boldsymbol{u}_K^n\big|^2 + \frac{1}{2\,|K|}\sum_{\sigma=K|L}\Big(\big|\tilde{\boldsymbol{u}}_{\sigma,cv}^{n+1}\big|^2 - \big|\tilde{\boldsymbol{u}}_K^{n+1}\big|^2\Big)\,F_{K,\sigma}^n$$
$$- \frac{1}{2\,|K|}\sum_{\sigma=K|L}\big|\tilde{\boldsymbol{u}}_{\sigma,cv}^{n+1} - \tilde{\boldsymbol{u}}_K^{n+1}\big|^2 F_{K,\sigma}^n + \widetilde{\boldsymbol{\nabla}_K\, p^n}\cdot\tilde{\boldsymbol{u}}_K^{n+1} = 0.$$

Multiplying the mass balance (26) *by* $\frac{1}{2}\big|\tilde{\boldsymbol{u}}_K^{n+1}\big|^2$ *and adding to this latter equation yields:*

$$\frac{1}{2\delta t}\Big(\rho_K^n\big|\tilde{\boldsymbol{u}}_K^{n+1}\big|^2 - \rho_K^{n-1}\big|\boldsymbol{u}_K^n\big|^2\Big) + \frac{1}{2\,|K|}\sum_{\sigma=K|L}\big|\tilde{\boldsymbol{u}}_{\sigma,cv}^{n+1}\big|^2 F_{K,\sigma}^n + \widetilde{\boldsymbol{\nabla}_K\, p^n}\cdot\tilde{\boldsymbol{u}}_K^{n+1}$$
$$= -\frac{1}{2\delta t}\rho_K^{n-1}\big|\tilde{\boldsymbol{u}}_K^{n+1} - \boldsymbol{u}_K^n\big|^2 + \frac{1}{2\,|K|}\sum_{\sigma=K|L}\big|\tilde{\boldsymbol{u}}_{\sigma,cv}^{n+1} - \tilde{\boldsymbol{u}}_K^{n+1}\big|^2 F_{K,\sigma}^n. \quad (27)$$

The velocity update (20a) *in the correction step can be rewritten as:*

$$\frac{1}{\delta t}\sqrt{\rho_K^n}\boldsymbol{u}_K^{n+1} + \frac{1}{\sqrt{\rho_K^n}}\boldsymbol{\nabla}_K\, p^{n+1} = \frac{1}{\delta t}\sqrt{\rho_K^n}\tilde{\boldsymbol{u}}_K^{n+1} + \frac{1}{\sqrt{\rho_K^n}}\widetilde{\boldsymbol{\nabla}_K\, p^n}.$$

Taking the square of this equality and multiplying by $\frac{\delta t}{2}$*, we get:*

$$\frac{1}{2\delta t}\rho_K^n\big|\tilde{\boldsymbol{u}}_K^{n+1}\big|^2 + \tilde{\boldsymbol{u}}_K^{n+1}\cdot\widetilde{\boldsymbol{\nabla}_K\, p^n} = \frac{1}{2\delta t}\rho_K^n\big|\boldsymbol{u}_K^{n+1}\big|^2 + \boldsymbol{u}_K^{n+1}\cdot\boldsymbol{\nabla}_K\, p^{n+1} + P_K^{n+1}, \quad (28)$$

where P_K^{n+1} *is defined by* (25)*. Using this relation in* (27) *yields the following discrete kinetic energy balance:*

$$\frac{1}{2\delta t}\Big(\rho_K^n\big|\boldsymbol{u}_K^{n+1}\big|^2 - \rho_K^{n-1}\big|\boldsymbol{u}_K^n\big|^2\Big) + \frac{1}{2\,|K|}\sum_{\sigma=K|L}\big|\tilde{\boldsymbol{u}}_{\sigma,cv}^{n+1}\big|^2 F_{K,\sigma}^n + \boldsymbol{\nabla}_K\, p^{n+1}\cdot\boldsymbol{u}_K^{n+1}$$
$$= -\frac{1}{2\delta t}\rho_K^{n-1}\big|\tilde{\boldsymbol{u}}_K^{n+1} - \boldsymbol{u}_K^n\big|^2 + \frac{1}{2\,|K|}\sum_{\sigma=K|L}\big|\tilde{\boldsymbol{u}}_{\sigma,cv}^{n+1} - \tilde{\boldsymbol{u}}_K^{n+1}\big|^2 F_{K,\sigma}^n - P_K^{n+1}.$$

In the centered case, $2\tilde{\boldsymbol{u}}_{\sigma,cv}^{n+1} = \tilde{\boldsymbol{u}}_K^{n+1} + \tilde{\boldsymbol{u}}_L^{n+1}$*, and the flux terms on the left and the right hand side can be combined to yield:*

$$\frac{1}{2\delta t}\Big(\rho_K^n\,\big|\boldsymbol{u}_K^{n+1}\big|^2 - \rho_K^{n-1}\,\big|\boldsymbol{u}_K^n\big|^2\Big) + \frac{1}{2\,|K|}\sum_{\sigma=K|L}\tilde{\boldsymbol{u}}_K^{n+1}\cdot\tilde{\boldsymbol{u}}_L^{n+1}F_{K,\sigma}^n + \boldsymbol{\nabla}_K\, p^{n+1}\cdot\boldsymbol{u}_K^{n+1} = R_{ctr,K}^{n+1} - P_K^{n+1}$$

with

$$R_{ctr,K}^{n+1} = -\frac{1}{2\delta t}\rho_K^{n-1}\,\big|\tilde{\boldsymbol{u}}_K^{n+1} - \boldsymbol{u}_K^n\big|^2.$$

In the upwind case, i.e. $\tilde{\boldsymbol{u}}_{\sigma,cv}^{n+1} = \tilde{\boldsymbol{u}}_K^{n+1}$ *if* $F_{K,\sigma}^n > 0$ *and* $\tilde{\boldsymbol{u}}_{\sigma,cv}^{n+1} = \tilde{\boldsymbol{u}}_L^{n+1}$ *if* $F_{K,\sigma}^n \leqslant 0$*, the flux at the right-hand side simplifies to give:*

$$\frac{1}{2\delta t}\Big(\rho_K^n\big|\boldsymbol{u}_K^{n+1}\big|^2 - \rho_K^{n-1}\big|\boldsymbol{u}_K^n\big|^2\Big) + \frac{1}{2\,|K|}\sum_{\sigma=K|L}\big|\tilde{\boldsymbol{u}}_{\sigma,cv}^{n+1}\big|^2 F_{K,\sigma}^n + \boldsymbol{\nabla}_K\, p^{n+1}\cdot\boldsymbol{u}_K^{n+1} = R_{upw,K}^{n+1} - P_K^{n+1},$$

with:

$$R_{upw,K}^{n+1} = -\frac{1}{2\delta t}\rho_K^{n-1}\big|\tilde{\boldsymbol{u}}_K^{n+1} - \boldsymbol{u}_K^n\big|^2 - \frac{1}{2\,|K|}\sum_{\sigma=K|L}\big|\tilde{\boldsymbol{u}}_L^{n+1} - \tilde{\boldsymbol{u}}_K^{n+1}\big|^2\big(F_{K,\sigma}^n\big)^-.$$

We conclude the proof by recasting R_K^{n+1} *under the form of* (24)*.*

Remark 3.4 (Well posedness of the prediction step) *The momentum balance* (18)-(19) *of the prediction step yields a linear system for the unknowns* $(\widetilde{\boldsymbol{u}}_K^{n+1})_{K\in\mathcal{M}}$. *The corresponding homogeneous system reads*

$$\frac{1}{\delta t}\rho_K^n\ \tilde{\boldsymbol{u}}_K^{n+1} + \mathbf{div}_K(\rho^n \boldsymbol{u}^n \otimes \tilde{\boldsymbol{u}}^{n+1}) = 0.$$

Estimate (27) *established in the above proof applied to this homogeneous system (i.e. setting* $\boldsymbol{u}_K^n$ *and* $\widetilde{\boldsymbol{\nabla}_K p^n}$ *to zero) yields, multiplying by* $|K|$ *and summing over* $K\in\mathcal{M}$,

$$\frac{1}{\delta t}\sum_{K\in\mathcal{M}}|K|\rho_K^n\big|\tilde{\boldsymbol{u}}_K^{n+1}\big|^2 + \frac{1}{2}\sum_{K\in\mathcal{M}}\sum_{\sigma=K|L}\big|\tilde{\boldsymbol{u}}_{\sigma,cv}^{n+1}\big|^2 F_{K,\sigma}^n = \frac{1}{2}\sum_{K\in\mathcal{M}}\sum_{\sigma=K|L}\big|\tilde{\boldsymbol{u}}_{\sigma,cv}^{n+1} - \tilde{\boldsymbol{u}}_K^{n+1}\big|^2 F_{K,\sigma}^n.$$

Thanks to the conservativity of the fluxes, the second term of the left-hand side vanishes, while the right-hand side is zero in the centered case and non-positive in the upwind case. Hence,

$$\frac{1}{\delta t}\sum_{K\in\mathcal{M}}|K|\ \rho_K^n\ \big|\tilde{\boldsymbol{u}}_K^{n+1}\big|^2 \leqslant 0,$$

which, since the density is positive, shows that the solution of this system is the null vector. The prediction step is thus well-posed.

The pressure correction scheme on staggered grids was proven to preserve the overall total energy balance [20, 21] (*i.e.* the integral of this relation over the space domain). Thanks to the colocated feature of the present scheme, it is easy to prove here that the total energy balance is conserved locally.

Proposition 3.5 (Local total energy balance) *Assume that* $\wp$ *is given by* (2), *that* $\rho_0 > 0$ *and* $e_0 \geqslant 0$, *and that* $\{\rho_K^n, e_K^n, \boldsymbol{u}_K^n,\ K\in\mathcal{M},\ n\in[\![0,N]\!]\}$ *is a solution to the scheme* (17)–(20). *Then the following local total energy balance holds for all* $K\in\mathcal{M}$ *and* $n\in[\![0,N-1]\!]$*:*

$$\frac{1}{\delta t}\big((\widetilde{\rho_K E_K})^{n+1} - (\widetilde{\rho_K E_K})^n\big) + \mathrm{div}_K(\rho^{n+1}e^{n+1}\boldsymbol{u}^{n+1}) + \frac{1}{2\,|K|}\sum_{\sigma=K|L}\tilde{\boldsymbol{u}}_{\sigma,K}^{n+1}\cdot\tilde{\boldsymbol{u}}_{\sigma,L}^{n+1}F_{K,\sigma}^n + \mathrm{div}_K(p^{n+1}\boldsymbol{u}^{n+1}) + P_K^{n+1} = 0, \quad (29)$$

where $\tilde{\boldsymbol{u}}_{\sigma,K}^{n+1}$ *and* $\tilde{\boldsymbol{u}}_{\sigma,L}^{n+1}$ *are defined by* (23), $\mathrm{div}_K(p^{n+1}\boldsymbol{u}^{n+1})$ *is defined by* (10), P_K^{n+1} *is defined by* (25) *and*

$$(\widetilde{\rho_K E_K})^n = \rho_K^n e_K^n + \frac{1}{2}\rho_K^{n-1}|\boldsymbol{u}_K^n|^2. \quad (30)$$

Proof 4 *From the definition of the terms* R_K^{n+1} *and* S_K^{n+1}, *summing the kinetic energy balance given by* (22) *with the internal energy balance (20c) and using the property* (10) *yields the total energy balance.*

Remark 3.6 (On the scaling of the pressure gradient) *The scaling of the pressure gradient* (20a) *appearing in the momentum balance* (18) *(and subsequently in the velocity update) is chosen such that the term* P_K^n *defined by* (25) *appears to be the difference of a same quantity written at two successive time steps; this allows to obtain the weak consistency of the total energy (see the proof of Theorem 4.5) from the local total energy balance*(29). *To explain this choice, let us write the scaling* (19) *as* $\widetilde{\boldsymbol{\nabla}_K p^n} = a_K^n\,\boldsymbol{\nabla}_K p^n$ *with* $a_K^n\in\mathbb{R}$. *Then the term* P_K *appearing in* (28) *becomes:*

$$P_K = \frac{\delta t}{2\,|K|}\Big[\underbrace{\frac{1}{\rho_K^n}}_{b_K^{n+1}}\,|\,\boldsymbol{\nabla}_K p^{n+1}|^2 - \underbrace{\frac{(a_K^n)^2}{\rho_K^n}}_{b_K^n}\,|\,\boldsymbol{\nabla}_K p^n|^2\Big].$$

which takes the desired form if $b_K^n = 1/\rho_K^{n-1} = (a_K^n)^2/\rho_K^n$, *that is* $a_K^n = \sqrt{\rho_K^n}/\sqrt{\rho_K^{n-1}}$, *hence the choice of the scaling* (19). *This technique is quite general (in the sense that it does not depend on the discretisation), as shown in the time semi-discrete setting in Appendix A of [15].*

Remark 3.7 (Presentation of the scheme as a discretisation of the conservative equations) *Instead of discretising the internal energy balance, we could have equivalently introduced the scheme by stating the discrete total energy balance* (29), *and thus presenting the algorithm as a conservative approximation of the (conservative) Euler equations. Then, deriving the kinetic energy balance and subtracting yields a discrete internal energy balance, whose expression ensures that this latter quantity remains positive. This computation justifies the definition* (30) *of the discrete total energy and the expression of the convective fluxes in* (29), *both being rather non-standard.*

An entropy for the Euler system with a perfect gas EOS is given by the function $\eta : \mathbb{R}_+^* \times \mathbb{R}_+^* \to \mathbb{R}$ defined by

$$\eta(\rho, e) = \rho \ln(\rho) - \frac{1}{\gamma - 1} \rho \ln e. \tag{31}$$

Indeed, formally, the following entropy inequality holds

$$\partial_t \eta(\rho, e) + \operatorname{div}\big[\eta(\rho, e)\, \boldsymbol{u}\big] \leqslant 0.$$

The scheme satisfies an analogous entropy inequality, stated in the following lemma; this result is an immediate consequence of [13, Theorem 2.3].

Lemma 3.8 (Discrete entropy inequality) *Any solution of the scheme* (16) *or* (20) *satisfies, for any* $K \in \mathcal{M}$ *and* $0 \leqslant n \leqslant N-1$*:*

$$\frac{|K|}{\delta t}(\eta_K^{n+1} - \eta_K^n) + \sum_{\sigma \in \mathcal{E}(K)} |\sigma|\ \eta_\sigma^{n+1} u_{K,\sigma}^{n+1} \leqslant 0, \tag{32}$$

with $\eta_K^m = \rho_K^m \ln(\rho_K^m) - \frac{1}{\gamma-1}\rho_K^m \ln e_K^m$, $m = n,\ n+1$, *and* $\eta_\sigma^{n+1} = \rho_\sigma^{n+1} \ln(\rho_\sigma^{n+1}) - \frac{1}{\gamma-1}\rho_\sigma^{n+1} \ln e_\sigma^{n+1}$.

Even though this inequality is not an estimate on the approximate solution, it is useful in order to prove that if a sequence of approximate solutions to the implicit scheme (16) or the pressure correction scheme (20) converges, then its limit is an entropy weak solution of the Euler system, see Theorem 4.5 below.

The proof of existence of a solution to the non-linear projection step relies on the topological degree theory, see e.g. [6] for the theory and [9, chapter 6], for an application to finite volume discretisations of PDEs. We proceed here as in [9, section 6.4.1].

Theorem 3.9 (Existence of a solution to the scheme) *Under the assumptions of Proposition 3.5, there exists a solution to the scheme* (18)–(20d).

Proof 5 *We proceed by induction. Let us assume the existence of a solution up to* t_n, *i.e. the existence of* $(\rho_K^k, p_K^k, \tilde{\boldsymbol{u}}_K^k, \boldsymbol{u}_K^k, e_K^k)_{K\in\mathcal{M}}$ *for* $0 \leqslant k \leqslant n$, *and let us prove the existence of* $(\rho_K^{n+1}, p_K^{n+1}, \tilde{\boldsymbol{u}}_K^{n+1}, \boldsymbol{u}_K^{n+1}, e_K^{n+1})_{K\in\mathcal{M}}$. *We already showed in Remark 3.4 the well-posedness of the prediction step. Let us now prove the existence of a solution* $(\rho_K^{n+1}, p_K^{n+1}, \boldsymbol{u}_K^{n+1}, e_K^{n+1})_{K\in\mathcal{M}}$ *to* (20a)–(20d). *Let* λ *be a real number in* $[0,1]$. *We consider the following non-linear system of equations:*

$$U_{\mathcal{M}}^{n+1} + \lambda \mathcal{F}(U_{\mathcal{M}}^{n+1}) = V_{\mathcal{M}}^n \tag{33}$$

where $U_{\mathcal{M}}^{n+1}$ *and* $V_{\mathcal{M}}^n$ *are vectors of* $\mathbb{R}^M$, $M = (2+d)\ \mathrm{card}(\mathcal{M})$, *defined by*

$$U_{\mathcal{M}}^{n+1} = \big[(\boldsymbol{u}_K^{n+1})_{K\in\mathcal{M}}^t,\ (\rho_K^{n+1})_{K\in\mathcal{M}},\ (\rho_K^{n+1} e_K^{n+1})_{K\in\mathcal{M}}\big]^t,$$

$$V_{\mathcal{M}}^n = \big[(\tilde{\boldsymbol{u}}_K^{n+1})_{K\in\mathcal{M}}^t,\ (\rho_K^n)_{K\in\mathcal{M}},\ (\rho_K^n e_K^n)_{K\in\mathcal{M}}\big]^t,$$

and

$$\mathcal{F}(U_{\mathcal{M}}^{n+1}) = \delta t \begin{bmatrix} \dfrac{1}{\rho_K^n}\Big(\nabla_K p^{n+1} - \widetilde{\nabla_K p^n}\Big) \\ \mathrm{div}_K(\rho^{n+1}\boldsymbol{u}^{n+1}) \\ \mathrm{div}_K(\rho^{n+1}e^{n+1}\boldsymbol{u}^{n+1}) + p_K^{n+1}\,\mathrm{div}_K\,\boldsymbol{u}^{n+1} - S_K^{n+1} \end{bmatrix}$$

with $p_K^{n+1} = (\gamma-1)\,\rho_K^{n+1}e_K^{n+1}$ *and* S_K^{n+1} *defined by* (21). *For* $\lambda = 1$, *the system* (33) *is the original projection-correction step. For* $\lambda = 0$, *it is a (trivially) invertible linear system. By the same arguments as in the proof of Proposition 3.2, we get that* $\rho_K^{n+1} > 0$ *and* $e_K^{n+1} \geqslant 0$, *for any* $\lambda \in [0,1]$. *Moreover, multiplying the second equation of* (33) *by* $|K|$ *and summing over all* $K \in \mathcal{M}$, *we get by conservativity:*

$$\sum_{K\in\mathcal{M}} |K|\,\rho_K^{n+1} = \sum_{K\in\mathcal{M}} |K|\,|\rho_K^{n+1}| = \sum_{K\in\mathcal{M}} |K|\,\rho_K^n, \tag{34}$$

which yields a uniform (in λ*) estimate on* ρ_K^{n+1}. *Let us then take the inner product of the first equation of* (33) *with* $|K|\,\rho_K^n\boldsymbol{u}_K^{n+1}$, *to get:*

$$|K|\,\rho_K^n|\boldsymbol{u}_K^{n+1}|^2 + \frac{\lambda}{\delta t}|K|\,\nabla_K p^{n+1}\cdot\boldsymbol{u}_K^{n+1} = |K|\,\rho_K^n\tilde{\boldsymbol{u}}_K^{n+1}\cdot\boldsymbol{u}_K^{n+1} + \frac{\lambda}{\delta t}|K|\,\widetilde{\nabla_K p^n}\cdot\boldsymbol{u}_K^{n+1}.$$

By Young's inequality, we thus get:

$$\frac{1}{2}|K|\,\rho_K^n|\boldsymbol{u}_K^{n+1}|^2 + \frac{\lambda}{\delta t}|K|\,\nabla_K p^{n+1}\cdot\boldsymbol{u}_K^{n+1} \leqslant C_K$$

where C_K *only depends on quantities which are known at this stage. Summing with the third equation of* (33) *multiplied by* $|K|$ *and then summing the resulting relation over the mesh and invoking the discrete* $\boldsymbol{\nabla} - \mathrm{div}$ *duality and the conservativity, we obtain the following uniform (in* λ*) estimate:*

$$\sum_{K\in\mathcal{M}} |K|\,\Big(|\rho_K^{n+1}e_K^{n+1}| + \frac{1}{2}\rho_K^n\,|\boldsymbol{u}_K^{n+1}|^2\Big) \leqslant C, \tag{35}$$

where $C \geqslant 0$ *once again only depends on known quantities. The mapping* $\mathcal{H}(\lambda,\cdot) = Id - \lambda\mathcal{F}$ *defines a homotopy between the mapping* $\mathcal{H}(1,\cdot)$ *associated with the original system* $U_{\mathcal{M}}^{n+1} + \mathcal{F}(U_{\mathcal{M}}^{n+1}) = V_{\mathcal{M}}^n$ *and the identity function* $\mathcal{H}(0,\cdot)$. *Thanks to the uniform estimates* (34) *and* (35), *we can then define a closed ball* $\mathcal{B}$ *of* $\mathbb{R}^M$ *with radius large enough so that the possible solutions of Problem* (33) *(including* $V_{\mathcal{M}}^n$ *which is obtained for* $\lambda = 0$*) lie in the interior of* $\mathcal{B}$. *Let us consider the topological degree* $deg(\mathcal{H}(\lambda,\cdot),\mathcal{B},V_{\mathcal{M}}^n)$ *of the map* $\mathcal{H}(\lambda,\cdot)$ *on the set* $\mathcal{B}$. *Using the invariance of the topological degree for a homotopy, we have:*

$$deg(\mathcal{H}(1,\cdot),\mathcal{B},V_{\mathcal{M}}^n) = deg(\mathcal{H}(0,\cdot),\mathcal{B},V_{\mathcal{M}}^n) = deg(Id,\mathcal{B},V_{\mathcal{M}}^n) = 1.$$

As a result, the non-linear problem obtained for $\lambda = 1$ *has at least one solution in* $\mathcal{B}$, *which concludes the proof.*

4. Passing to the limit in the scheme

In this section, we show that any possible limit of a sequence of discrete solutions to the pressure-correction scheme obtained with a sequence of meshes and time steps such that the space and time steps tend to zero satisfies the weak form of the continuous problem. In some respect, it means that the shocks are correctly computed by the pressure-correction scheme, since the Rankine-Hugoniot conditions are derived from the weak form of the Euler equations. Furthermore, any such possible limit is shown to satisfy a weak entropy inequality. The convergence analysis is performed for the mesh size $h_{\mathcal{M}}$ of the mesh $\mathcal{M}$ tending to 0; the mesh size $h_{\mathcal{M}}$ is defined by:

$$h_{\mathcal{M}} = \sup_{K\in\mathcal{M}} h_K, \text{ with } h_K = \mathrm{diam}(K).$$

Discrete unknown functions and norms – Let $\mathcal{M}$ be a finite volume mesh of Ω as defined in Section 2.1. To a set of discrete scalar of vector field $(z_K)_{K\in\mathcal{M}}$, we associate the piecewise constant function $z_\mathcal{M} : \Omega \to \mathbb{R}$ or $\mathbb{R}^d$ defined by:

$$z_\mathcal{M}(\boldsymbol{x}) = \sum_{K\in\mathcal{M}} z_K \ \mathbb{1}_K(\boldsymbol{x}), \quad \forall \boldsymbol{x} \in \Omega,$$

where, for any set $A \subset \mathbb{R}^d$, the function $\mathbb{1}_A$ is the characteristic function of A defined by $\mathbb{1}_A(\boldsymbol{x}) = 1$ if $\boldsymbol{x} \in A$, $\mathbb{1}_A(\boldsymbol{x}) = 0$ otherwise. We denote by $L_\mathcal{M}$ the set of piecewise constant functions on $\mathcal{M}$. We define a BV discrete semi-norm of a function $z_\mathcal{M} \in L_\mathcal{M}$ by:

$$|z_\mathcal{M}|_{BV_x} = \sum_{\substack{\sigma\in\mathcal{E}_{\rm int}\\ \sigma=K|L}} |\sigma| \ |z_L - z_K|. \tag{36}$$

Let $(\mathcal{M}, \delta t)$ be a space-time discretisation. To a set of discrete values $\{z_K^n,\ K \in \mathcal{M},\ n \in [\![0, N]\!]\}$, we associate the following piecewise constant function of time and space:

$$z_{\mathcal{M},\delta t}(\boldsymbol{x}, t) = \sum_{n=0}^{N-1} \sum_{K\in\mathcal{M}} z_K^{n+1} \ \mathbb{1}_K(\boldsymbol{x}) \ \mathbb{1}_n(t), \quad \forall \boldsymbol{x} \in \Omega,\ \forall t \in [0, T),$$

where, for short, $\mathbb{1}_n$ stands for the characteristic function of the time interval $(t_n, t_{n+1}]$. We define the following BV discrete semi-norm:

$$|z_{\mathcal{M},\delta t}|_{L^1(BV_x)} = \sum_{n=0}^{N} \delta t \ |z^n_{\mathcal{M},\delta t}|_{BV_x},$$

Given a solution $\{\rho_K^n, \boldsymbol{u}_K^n, e_K^n,\ K \in \mathcal{M},\ n \in [\![0, N]\!]\}$ of the scheme (17)–(20), we may thus define the piecewise constant functions $\rho_{\mathcal{M},\delta t}$, $p_{\mathcal{M},\delta t}$, $\boldsymbol{u}_{\mathcal{M},\delta t}$, $e_{\mathcal{M},\delta t}$ and their BV semi-norm.

Interpolates and discrete derivative operators – Let $\varphi \in C_c^\infty(\Omega \times [0, T))$ be a given test function. We denote by $\varphi_{\mathcal{M},\delta t}$ its interpolate for the space–time discretisation $(\mathcal{M}, \delta t)$, defined by:

$$\varphi_{\mathcal{M},\delta t}(\boldsymbol{x}, t) = \sum_{n=0}^{N-1} \sum_{K\in\mathcal{M}} \varphi_K^n \ \mathbb{1}_K(\boldsymbol{x}) \ \mathbb{1}_n(t), \text{ with } \varphi_K^n = \varphi(\boldsymbol{x}_K, t_n),\ \forall K \in \mathcal{M},\ \forall n \in [\![0, N-1]\!]. \tag{37}$$

The interpolate $\boldsymbol{\varphi}_{\mathcal{M},\delta t}$ of a vector-valued test function $\boldsymbol{\varphi} \in C_c^\infty(\Omega \times [0, T))^d$ is then the vector valued function whose components are the interpolates of the components of $\boldsymbol{\varphi}$. We may then define a discrete time-derivative operator $\eth_t$ by:

$$\eth_t \varphi_{\mathcal{M},\delta t}(\boldsymbol{x}, t) = \sum_{n=0}^{N-1} \sum_{K\in\mathcal{M}} \frac{\varphi_K^{n+1} - \varphi_K^n}{\delta t} \ \mathbb{1}_K(\boldsymbol{x}) \ \mathbb{1}_n(t),\ \forall \boldsymbol{x} \in \Omega,\ \forall t \in [0, T).$$

Owing to the regularity of φ, the quantity $\eth_t \varphi_{\mathcal{M},\delta t}$ converges uniformly to $\partial_t \varphi$ as the space and time steps tend to 0. It is also convenient in the convergence analysis to define a discrete gradient of $\varphi_{\mathcal{M},\delta t}$ on a dual mesh which is composed of the so called "diamond cells", represented on Figure 2 and defined as follows. For a control volume $K \in \mathcal{M}$, $\sigma \in \mathcal{E}(K)$, we define the half-diamond cell $D_{K,\sigma}$ as the cone with basis σ and vertex $\boldsymbol{x}_K$:

$$D_{K,\sigma} = \big\{t\boldsymbol{x}_K + (1-t)\boldsymbol{y},\ t \in [0, 1],\ \boldsymbol{y} \in \sigma\big\}. \tag{38}$$

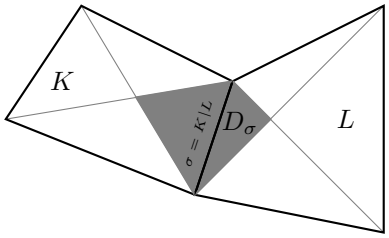

FIG. 2. A dual mesh and cell.

We then define the diamond cells D_σ as

$$D_\sigma = \begin{cases} D_{K,\sigma} \cup D_{L,\sigma} \text{ if } \sigma = K|L \in \mathcal{E}_{\rm int}, \\ D_{K,\sigma} \text{ if } \sigma \in \mathcal{E}_{\rm ext} \text{ and } \sigma \in \mathcal{E}(K). \end{cases} \tag{39}$$

We denote by $|D_{K,\sigma}|$ and $|D_\sigma|$ the d-dimensional measure of $D_{K,\sigma}$ and D_σ, respectively. The dual mesh regularity is defined by:

$$\eta_{\mathcal{M}} = \max\Big\{ \frac{|D_\sigma|}{|D_{K,\sigma}|},\ K \in \mathcal{M},\ \sigma \in \mathcal{E}(K) \Big\}. \tag{40}$$

A discrete gradient operator $\nabla_{\mathcal{E}} z_{\mathcal{M}}$ of a piecewise constant function $z_{\mathcal{M}} \in L_{\mathcal{M}}$ may then be defined as the following piecewise constant function on the dual mesh:

$$\nabla_{\mathcal{E}} z_{\mathcal{M}} = \sum_{\substack{\sigma \in \mathcal{E}_{\rm int} \\ \sigma = K|L}} \frac{|\sigma|}{|D_\sigma|} (z_L - z_K)\, \boldsymbol{n}_{K,\sigma}\ \mathbb{1}_{D_\sigma}. \tag{41}$$

This discrete gradient is not consistent in general, in the sense that, applied to the interpolate of a smooth function, it converges only $\star$–weakly in $L^\infty(\Omega \times (0,T))$; this result may be related to the weak convergence of a discrete gradient proven in [8, Lemma 2] for meshes satisfying an orthogonality condition in the case $r = 2$ and of [28, Lemma 6.2] for quadrangular and hexahedral meshes, and any r. It is in fact valid for any kind of mesh under a regularity assumption, and was extended to time-dependent functions, see [11, Lemma 3.2]. We recall here this latter result for the sake of completeness.

Lemma 4.1 (Weak consistency of the face gradient) *Let $(\mathcal{M}^{(m)})_{m\in\mathbb{N}}$ be a sequence of meshes such that the mesh step $h_{\mathcal{M}^{(m)}}$ tends to zero when m tends to $+\infty$. Assume that there exists a real number θ^∇ such that*

$$\max_{\sigma \in \mathcal{E}_{\rm int}^{(m)}, \sigma = K|L} \frac{|\sigma|\ |\boldsymbol{x}_L - \boldsymbol{x}_K|}{|D_\sigma|} \leqslant \theta^\nabla, \forall m \in \mathbb{N}. \tag{42}$$

For $m \in \mathbb{N}$, we suppose given a time step $\delta t^{(m)}$, and suppose that $\delta t^{(m)}$ also tends to zero when m tends to $+\infty$. Let $\varphi \in C_c^\infty(\Omega \times [0,T])$ and, for $m \in \mathbb{N}$, $\nabla^{(m)}\varphi \in L^\infty(\Omega \times [0,T])^d$ be defined by:

$$\nabla^{(m)}\varphi = \sum_{n=0}^{N} \sum_{\sigma \in \mathcal{E}_{\rm int}^{(m)}} \frac{|\sigma|}{|D_\sigma|}\ (\varphi_L^n - \varphi_K^n)\, \boldsymbol{n}_{K,\sigma} \mathbb{1}_{D_\sigma}(\boldsymbol{x}) \mathbb{1}_n(t). \tag{43}$$

Then the sequence $(\nabla^{(m)}\varphi)_{m\in\mathbb{N}}$ is bounded in $L^\infty(\Omega \times [0,T])^d$ uniformly with respect to m and converges to $\nabla\varphi$ in $L^\infty(\Omega \times [0,T])^d$ weak $\star$.

Boundedness assumptions for sequences of approximate solutions – Consider a sequence $(\mathcal{M}^{(m)}, \delta t^{(m)})_{m\in\mathbb{N}}$ of space-time discretisations of $\Omega\times[0,T)$. For $m\in\mathbb{N}$, let us denote by $(\rho^{(m)},\ p^{(m)},\ e^{(m)},\ \tilde{\boldsymbol{u}}^{(m)},\ \boldsymbol{u}^{(m)})$ the piecewise constant functions reconstructed from the solutions of the scheme (17)–(20) for $(\mathcal{M},\delta t)=(\mathcal{M}^{(m)},\delta t^{(m)})$. Let us introduce the following notation:

$$\|\frac{1}{\rho^{(m)}}\|_\infty = \max\{\frac{1}{(\rho^{(m)})^n_K},\ K\in\mathcal{M}^{(m)},\ n\in[\![-1,N^{(m)}]\!]\},$$

$$\|p^{(m)}\|_\infty = \max\{(p^{(m)})^n_K,\ K\in\mathcal{M}^{(m)},\ n\in[\![0,N^{(m)}]\!]\}.$$

In any other ocurrence, the notation $\|z\|_\infty$ stands for the usual L^∞ norm of the function z. For the consistency result stated above, we need to assume that there exists $C>0$ such that, for all $m\in\mathbb{N}$,

$$\|(\rho^{(m)})^0\|_\infty + |(\rho^{(m)})^0|_{BV_x} + \|(\boldsymbol{u}^{(m)})^0\|_\infty + |(\boldsymbol{u}^{(m)})^0|_{BV_x} \leqslant C, \tag{44}$$

$$\|\frac{1}{\rho^{(m)}}\|_\infty + \|p^{(m)}\|_\infty + |p^{(m)}|_{L^1(BV_x)} \leqslant C. \tag{45}$$

Note that the assumptions on the unknowns at the first time step imply that the BV-norm of the initial data for the density and the velocity is bounded.

Reconstruction of discrete functions – In order to alleviate the consistency proofs, some stability and convergence results on the reconstruction of approximate solutions on dual meshes are first introduced; these results are a rather straightforward extension to general meshes of those presented in [12, Lemmas 3.3 and 3.9] for rectangular meshes.

Lemma 4.2 (Dual mesh reconstruction: definition and stability) *Let $\mathcal{M}$ be a finite volume mesh of Ω as defined in Section 2.1 and let $\mathcal{T}$ be its dual mesh, formed with the dual cells defined by* (38)-(39)*. A reconstruction operator is an operator $\mathcal{R}_\mathcal{M}$ from the set $L_\mathcal{M}$ of piecewise constant functions on $\mathcal{M}$ to the set $L_\mathcal{T}$ of piecewise constant functions on $\mathcal{T}$, defined as follows:*

$$\mathcal{R}_\mathcal{M}: \quad \left|\begin{array}{lcl} L_\mathcal{M} & \to & L_\mathcal{T} \\ z_\mathcal{M} & \mapsto & \mathcal{R}_\mathcal{M} z_\mathcal{M} = \displaystyle\sum_{\sigma\in\mathcal{E}} \widehat{z}_\sigma\ \mathbb{1}_{D_\sigma}, \end{array}\right.$$

where $\widehat{z}_\sigma$ is a convex combination of the values of the neighbouring cells, i.e.

$$\widehat{z}_\sigma = \begin{cases} \mu_\sigma\, z_K + (1-\mu_\sigma)\, z_L \ \text{if } \sigma = K|L\in\mathcal{E}_{\rm int},\ \text{with } 0\leqslant\mu_\sigma\leqslant 1 \\ z_K \ \text{if } \sigma\in\mathcal{E}_{\rm ext}, \sigma\in\mathcal{E}(K). \end{cases}$$

For any $r\in[1,+\infty)$, there exists $C_{\eta_\mathcal{M}}\geqslant 0$, depending only on r and on the regularity of the mesh $\eta_\mathcal{M}$ defined by (40)*, and non-decreasing with respect to $\eta_\mathcal{M}$, such that, for any $z_\mathcal{M}\in L_\mathcal{M}$,*

$$\|\mathcal{R}_\mathcal{M} z_\mathcal{M}\|_{L^r(\Omega)} \leqslant C_{\eta_\mathcal{M}}\ \|z_\mathcal{M}\|_{L^r(\Omega)}.$$

Proof 6 *Let $r\in[1,+\infty)$ and $z_\mathcal{M}\in L_\mathcal{M}$; by definition,*

$$\|\mathcal{R}_\mathcal{M} z_\mathcal{M}\|^r_{L^r(\Omega)} = \sum_{\sigma\in\mathcal{E}} |D_\sigma|\ |\widehat{z}_\sigma|^r = \sum_{\substack{\sigma\in\mathcal{E}_{\rm int}\\ \sigma=K|L}} |D_\sigma|\ \left|\mu_\sigma z_K + (1-\mu_\sigma) z_L\right|^r + \sum_{\substack{\sigma\in\mathcal{E}_{\rm ext}\\ \sigma\in\mathcal{E}(K)}} |D_\sigma|\ \left|z_K\right|^r.$$

Since $|\mu_\sigma|\leqslant 1$ and $(a+b)^r\leqslant 2^{r-1}(a^r+b^r)$, for $a,b\in[0,+\infty)$, we get:

$$\begin{aligned}\|\mathcal{R}_\mathcal{M} z_\mathcal{M}\|^r_{L^r(\Omega)} &\leqslant 2^{r-1} \sum_{\substack{\sigma\in\mathcal{E}_{\rm int}\\ \sigma=K|L}} |D_\sigma|\ \left(|z_K|^r + |z_L|^r\right) + \sum_{\substack{\sigma\in\mathcal{E}_{\rm ext}\\ \sigma\in\mathcal{E}(K)}} |D_\sigma|\ |z_K|^r \\ &\leqslant 2^{r-1} \sum_{K\in\mathcal{M}} \Big[\sum_{\sigma\in\mathcal{E}(K)} |D_\sigma|\Big]\ |z_K|^r \leqslant 2^{r-1}\eta_\mathcal{M} \sum_{K\in\mathcal{M}} |K|\ |z_K|^r,\end{aligned}$$

thanks to the definition (40) *of $\eta_\mathcal{M}$, which concludes the proof.*

The following lemma states that if a sequence of piecewise constant functions of the primal mesh tends to some function in L^r, then a sequence of reconstructions also converges to the same function in L^r. It can be proven exactly in the same way as in [12, Lemmas 3.3 and 3.9].

Lemma 4.3 (Convergence of the dual mesh reconstructions) *Let $(\mathcal{M}^{(m)})_{m\in\mathbb{N}}$ be a sequence of finite volume meshes such that $h_{\mathcal{M}^{(m)}} \to 0$ as $m \to +\infty$, and which is supposed to satisfy the following regularity assumption:*

$$\text{There exists } \eta > 0 \text{ such that } \eta_{\mathcal{M}^{(m)}} \leqslant \eta, \text{ for any } m \in \mathbb{N}. \tag{46}$$

with $\eta_{\mathcal{M}^{(m)}}$ defined by (40). Let $1 \leqslant r < +\infty$. Let $\bar{z} \in L^r(\Omega)$, and let $(z_{\mathcal{M}}^{(m)})_{m\in\mathbb{N}}$ be such that $z_{\mathcal{M}}^{(m)} \in L_{\mathcal{M}^{(m)}}$ for any $m \in \mathbb{N}$ and $z_{\mathcal{M}}^{(m)}$ converges to $\bar{z}$ as $m \to +\infty$ in $L^r(\Omega)$. Let $\mathcal{R}_{\mathcal{M}^{(m)}}$ be a reconstruction operator on the dual mesh, in the sense of Lemma 4.2.

Then $\mathcal{R}_{\mathcal{M}^{(m)}} z_{\mathcal{M}}^{(m)} \to \bar{z}$ in $L^r(\Omega)$ as $m \to +\infty$.

THE CONSISTENCY RESULT – To pass to the limit in the scheme, we use an assumption linking the mesh and the time step which we now state. For a finite volume mesh $\mathcal{M}$, let $\underline{h}_{\mathcal{M}}$ be defined by:

$$\underline{h}_{\mathcal{M}} = \min_{K\in\mathcal{M}} \frac{|K|}{|\partial K|}. \tag{47}$$

Note that the fact that the ratio $\underline{h}_{\mathcal{M}}/h_{\mathcal{M}}$ is small detects the presence of "flat" control volumes in the mesh (in other words, $|K|/|\partial K|$ is significantly lower than $\mathrm{diam}(K)$ when the control volume K is flat). Let us now consider a sequence of meshes $(\mathcal{M}^{(m)})_{m\in\mathbb{N}}$ and times steps $(\delta t^{(m)})_{m\in\mathbb{N}}$. Then the consistency proof given below requires the following condition:

$$\lim_{m\to\infty} \frac{(\delta t^{(m)})^2}{\underline{h}_{\mathcal{M}^{(m)}}} = 0. \tag{48}$$

This latter relation combines a regularity assumption on the sequence of meshes (it forbids increasingly flat control volumes as $m \to +\infty$) with a CFL-like condition, however less restrictive than usual (it involves δt^2 instead of δt), and rather natural in practice. It is used in the present analysis to control the residual terms of the discrete kinetic energy balance equation taking the form of the square of a discrete pressure H^1-norm (terms denoted by P_K^{n+1} in (25), see the proof of Lemma 4.6 below).

The following result states the weak convergence of the pressure gradient, and will be used in the proof of consistency of the scheme below.

Lemma 4.4 (Weak consistency of the gradient) *Let $(\mathcal{M}^{(m)}, \delta t^{(m)})_{m\in\mathbb{N}}$ be a sequence of discretisations such that $h^{(m)} = h_{\mathcal{M}^{(m)}}$ and $\delta t^{(m)}$ tend to 0 when $m \to \infty$ and which satisfy the regularity assumptions (42) and (46). Let $(p^{(m)})_{m\in\mathbb{N}}$ be a sequence of discrete pressures, associated to the sequence of discretisations $(\mathcal{M}^{(m)}, \delta t^{(m)})_{m\in\mathbb{N}}$ and let us suppose that $(p^{(m)})_{m\in\mathbb{N}}$ converges to $\bar{p}$ in $L^r(\Omega)$, for $1 \leqslant r < \infty$. Let $\varphi \in C_c^\infty(\Omega \times [0,T))$ be a given test function and let us denote its interpolate $\varphi_{\mathcal{M}^{(m)},\delta t^{(m)}}$ defined by (37) by $\varphi^{(m)}$. Then:*

$$\lim_{m\to+\infty} \sum_{n=0}^{N^{(m)}-1} \delta t^{(m)} \sum_{K\in\mathcal{M}^{(m)}} |K| \ \boldsymbol{\nabla}_K (p^{(m)})^{n+1} (\varphi^{(m)})_K^n = -\int_0^T \int_\Omega \bar{p} \ \boldsymbol{\nabla}\phi \ \mathrm{d}\boldsymbol{x}\,\mathrm{d}t. \tag{49}$$

Proof 7 *Dropping for short the exponents $^{(m)}$ whenever it does not hinder comprehension, let $T^{(m)}$ be the quantity at the left-hand side of (49), namely:*

$$T^{(m)} = \sum_{n=0}^{N-1} \delta t \sum_{K\in\mathcal{M}} |K| \ \boldsymbol{\nabla}_K p^{n+1} \varphi_K^n.$$

Let m be large enough so that φ vanishes on the boundary cells; using the definition (7) of the discrete gradient and reordering the summation, we get:

$$T^{(m)} = \sum_{n=0}^{N-1} \delta t \sum_{\substack{\sigma\in\mathcal{E}_{\rm int}\\ \sigma=K|L}} |\sigma|\ p_\sigma^{n+1}\ \boldsymbol{n}_{K,\sigma}\ (\varphi_K^n - \varphi_L^n) = \sum_{n=0}^{N-1} \delta t \sum_{\substack{\sigma\in\mathcal{E}_{\rm int}\\ \sigma=K|L}} |D_\sigma|\ p_\sigma^{n+1}\ \frac{|\sigma|}{|D_\sigma|}(\varphi_K^n - \varphi_L^n)\ \boldsymbol{n}_{K,\sigma},$$

where, for $\sigma = K|L$, $p_\sigma^{n+1} = \alpha_{L,\sigma}\, p_K^{n+1} + \alpha_{K,\sigma}\, p_L^{n+1}$. We thus obtain that there exists a dual mesh reconstruction $p_{\mathcal{E}}^{(m)}$ of the discrete function $p^{(m)}$ such that:

$$T^{(m)} = -\int_0^T \int_\Omega p_{\mathcal{E}}^{(m)}\ \nabla_{\mathcal{E}^{(m)}}\varphi^{(m)}\ \mathrm{d}\boldsymbol{x}\,\mathrm{d}t.$$

The conclusion follows by Lemma 4.3 and Lemma 4.1.

We are now in position to prove the following consistency result, which is the aim of this section.

Theorem 4.5 (Consistency of the pressure-correction scheme) *Let $(\mathcal{M}^{(m)}, \delta t^{(m)})_{m\in\mathbb{N}}$ be a sequence of discretisations such that $h^{(m)} = h_{\mathcal{M}^{(m)}}$ and $\delta t^{(m)}$ tend to 0 when $m\to\infty$, satisfying the regularity assumptions (42) and (46) and the CFL-like condition (48).*
For $m\in\mathbb{N}$, let $(\rho^{(m)}, p^{(m)}, \tilde{\boldsymbol{u}}^{(m)}, \boldsymbol{u}^{(m)}, e^{(m)})$ be the piecewise constant functions corresponding to the solution of the scheme (17)–(20) for $(\mathcal{M}, \delta t) = (\mathcal{M}^{(m)}, \delta t^{(m)})$; we assume that these functions satisfy (44) and (45), and that the sequence $(\rho^{(m)}, p^{(m)}, \tilde{\boldsymbol{u}}^{(m)}, \boldsymbol{u}^{(m)}, e^{(m)})_{m\in\mathbb{N}}$ converges in $L^r(\Omega\times(0,T))^{3+2d}$ for $1\leqslant r<\infty$ to a limit $(\bar\rho, \bar p, \bar{\tilde{\boldsymbol{u}}}, \bar{\boldsymbol{u}}, \bar e)\in L^\infty(\Omega\times(0,T))^{3+2d}$.
Then $\bar{\tilde{\boldsymbol{u}}} = \bar{\boldsymbol{u}}$ and $(\bar\rho, \bar p, \bar{\boldsymbol{u}}, \bar e)$ is a weak solution of the Euler equations, i.e. satisfies:

$$\begin{aligned}
&\forall \varphi\in C_c^\infty(\Omega\times[0,T)),\ \forall \boldsymbol{\varphi}\in C_c^\infty(\Omega\times[0,T))^d,\\
&\int_0^T\int_\Omega \left(\bar\rho\,\partial_t\varphi + \bar\rho\bar{\boldsymbol{u}}\cdot\nabla\varphi\right)\,\mathrm{d}\boldsymbol{x}\,\mathrm{d}t + \int_\Omega \rho_0(\boldsymbol{x})\,\varphi(\boldsymbol{x},0)\,\mathrm{d}\boldsymbol{x} = 0, \qquad (50)\\
&\int_0^T\int_\Omega \left(\bar\rho\bar{\boldsymbol{u}}\cdot\partial_t\boldsymbol{\varphi} + (\bar\rho\bar{\boldsymbol{u}}\otimes\bar{\boldsymbol{u}}) : \nabla\boldsymbol{\varphi}\right)\,\mathrm{d}\boldsymbol{x}\,\mathrm{d}t + \int_\Omega \rho_0(\boldsymbol{x})\,\boldsymbol{u}_0(\boldsymbol{x})\cdot\boldsymbol{\varphi}(\boldsymbol{x},0)\,\mathrm{d}\boldsymbol{x} = 0, \qquad (51)\\
&\int_0^T\int_\Omega \left(\bar\rho\bar E\,\partial_t\varphi + (\bar\rho\bar E + \bar p)\bar{\boldsymbol{u}}\cdot\nabla\varphi\right)\,\mathrm{d}\boldsymbol{x}\,\mathrm{d}t + \int_\Omega \rho_0(\boldsymbol{x})E_0(\boldsymbol{x})\,\varphi(\boldsymbol{x},0)\,\mathrm{d}\boldsymbol{x} = 0, \qquad (52)\\
&\bar E = \bar e + \frac{1}{2}|\bar{\boldsymbol{u}}|^2,\ E_0 = e_0 + \frac{1}{2}|\boldsymbol{u}_0|^2, \bar p = (\gamma-1)\bar\rho\bar e.
\end{aligned}$$

If we furthermore assume that there exists $C\in\mathbb{R}_+$ such that $\|\frac{1}{e^{(m)}}\|_\infty\leqslant C$, then $(\bar\rho, \bar p, \bar{\boldsymbol{u}}, \bar e)$ is an entropy weak solution, in the sense that it satisfies the following weak entropy inequality:

$$-\int_0^T\int_\Omega \eta(\bar\rho,\bar e)\,\partial_t\varphi + \eta(\bar\rho,\bar e)\,\bar{\boldsymbol{u}}\cdot\boldsymbol{\nabla}\varphi\ \mathrm{d}\boldsymbol{x}\,\mathrm{d}t - \int_\Omega \eta(\bar\rho,\bar e)(\boldsymbol{x},0)\ \varphi(\boldsymbol{x},0)\ \mathrm{d}\boldsymbol{x}\leqslant 0,$$
$$\text{for any function } \varphi\in C_c^\infty\big([0,T)\times\bar\Omega\big), \varphi\geqslant 0. \qquad (53)$$

Proof 8 *The proof is organized in several steps: we first show that the predicted and the end-of-step velocity converge to the same limit, then the convergence of the initial data for the density, and, finally, we pass to the limit in the equations of the scheme and in the discrete entropy inequality. Throughout the proof, for the sake of simplicity, we shall drop the exponent "(m)" associated to the sequence of discretisations when it does not hinder comprehension.*

Equality of the limits $\bar{\tilde{\boldsymbol{u}}}$ and $\bar{\boldsymbol{u}}$ – *Using the velocity update (20a) and the definition of*

the pressure gradient (8)*, we have:*

$$\begin{aligned}\int_0^T \int_\Omega |\tilde{\boldsymbol{u}} - \boldsymbol{u}| \, \mathrm{d}\boldsymbol{x}\, \mathrm{d}t &= \sum_{n=0}^{N-1} \delta t \sum_{K\in\mathcal{M}} |K| \, |\boldsymbol{u}_K^{n+1} - \tilde{\boldsymbol{u}}_K^{n+1}| \\ &= \sum_{n=0}^{N-1} \delta t \sum_{K\in\mathcal{M}} |K| \, \Big| \frac{\delta t}{\rho_K^n} \boldsymbol{\nabla}_K p^{n+1} - \frac{\delta t}{\sqrt{\rho_K^{n-1}\rho_K^n}} \boldsymbol{\nabla}_K p^n \Big| \\ &\leqslant \|\frac{1}{\rho}\|_\infty \sum_{n=0}^{N} 2\,\delta t^2 \sum_{K\in\mathcal{M}} \sum_{\sigma=K|L} |\sigma| \, |p_L^n - p_K^n| \\ &\leqslant 4\,\delta t \, \|\frac{1}{\rho}\|_\infty \, |p|_{L^1(BV_x)}.\end{aligned}$$

Thanks to the assumption (45)*, we may pass to the limit in the above inequality and obtain* $\tilde{\bar{\boldsymbol{u}}} = \bar{\boldsymbol{u}}$*.*

Initial condition for ρ – *In the prediction-correction algorithm, the discrete initial condition* ρ^0 *is not directly computed from the continuous initial condition* ρ_0 *but rather by the solution of a discrete mass balance, as specified by* (17)*; thus,*

$$\rho_K^0 - \frac{1}{|K|} \int_K \rho_0 \, \mathrm{d}\boldsymbol{x} = \delta t \, \mathrm{div}_K(\rho^0 \boldsymbol{u}^0).$$

Therefore,

$$\int_\Omega |\rho^0 - \rho_0| \, \mathrm{d}\boldsymbol{x} = \delta t \sum_{K\in\mathcal{M}} \Big| \sum_{\sigma\in\mathcal{E}(K)} |\sigma| \rho_\sigma^0 u_{K,\sigma}^0 \Big| \leqslant \delta t \, (T_1 + T_2)$$

with:

$$T_1 = \sum_{K\in\mathcal{M}} \Big| \sum_{\sigma\in\mathcal{E}(K)} |\sigma| \, (\rho_\sigma^0 - \rho_K^0) \, u_{K,\sigma}^0 \Big|, \; T_2 = \sum_{K\in\mathcal{M}} \rho_K^0 \Big| \sum_{\sigma\in\mathcal{E}(K)} |\sigma| \, (u_{K,\sigma}^0 - \boldsymbol{u}_K^0 \cdot \boldsymbol{n}_{K,\sigma}) \Big|.$$

The first term may be estimated by $T_1 \leqslant 2 \, ||\boldsymbol{u}^0||_\infty |\rho^0|_{BV_x}$*. Moreover*

$$T_2 \leqslant \sum_{K\in\mathcal{M}} \rho_K^0 \sum_{\sigma=K|L} |\sigma| \, \big|(\alpha_{K,\sigma}\boldsymbol{u}_K^0 + \alpha_{L,\sigma}\boldsymbol{u}_L^0) - \boldsymbol{u}_K^0\big| \leqslant \sum_{K\in\mathcal{M}} \rho_K^0 \sum_{\sigma=K|L} |\sigma| \, \big|\boldsymbol{u}_L^0 - \boldsymbol{u}_K^0\big| \leqslant 2 \, ||\rho^0||_\infty \, |\boldsymbol{u}^0|_{BV_x}.$$

Consequently, $\displaystyle\int_\Omega |\rho^0 - \rho_0| \, \mathrm{d}\boldsymbol{x} \to 0$ *as* $\delta t \to 0$*, thanks to assumption* (44)*.*

Passage to the limit in the equations of the scheme – *Let* $\varphi \in C_c^\infty(\Omega \times [0,T))$ *and* $\boldsymbol{\varphi} \in C_c^\infty(\Omega \times [0,T))^d$*. For a given discretisation* $(\mathcal{M}^{(m)}, \delta t^{(m)})$*, the interpolates* $\varphi_{\mathcal{M}^{(m)},\delta t^{(m)}}$ *and* $\boldsymbol{\varphi}_{\mathcal{M}^{(m)},\delta t^{(m)}}$ *of* φ *and* $\boldsymbol{\varphi}$ *defined by* (37) *are respectively denoted by* $\varphi^{(m)}$ *and* $\boldsymbol{\varphi}^{(m)}$*.*

Mass balance – Let us now prove that $(\bar{\rho}, \bar{\boldsymbol{u}})$ *satisfies the mass balance equation* (50)*. Multiplying* (20b) *by* $\delta t \varphi_K^n$ *and summing for* $n \in [\![0, N-1]\!]$ *and* $K \in \mathcal{M}$ *yields* $T_1^{(m)} + T_2^{(m)} = 0$ *with*

$$T_1^{(m)} = \sum_{n=0}^{N-1} \sum_{K\in\mathcal{M}} |K| \, \left(\rho_K^{n+1} - \rho_K^n\right) \varphi_K^n, \quad T_2^{(m)} = \sum_{n=0}^{N-1} \delta t \sum_{K\in\mathcal{M}} \sum_{\sigma\in\mathcal{E}(K)} F_{K,\sigma}^{n+1} \varphi_K^n.$$

Reordering the summation in $T_1^{(m)}$ *and using the fact that* $\varphi^{N-1} = 0$ *at least for* m *large enough,*

we get

$$
\begin{aligned}
T_1^{(m)} &= -\sum_{n=0}^{N-1}\delta t\sum_{K\in\mathcal{M}}|K|\ \rho_K^{n+1}\frac{\varphi_K^{n+1}-\varphi_K^n}{\delta t}-\sum_{K\in\mathcal{M}}|K|\ \rho_K^0\varphi_K^0\\
&= -\int_0^T\int_\Omega \rho^{(m)}\eth_t\varphi^{(m)}\ \mathrm{d}\boldsymbol{x}\,\mathrm{d}t-\int_\Omega\left(\rho^{(m)}\right)^0\varphi^{(m)}(\boldsymbol{x},0)\ \mathrm{d}\boldsymbol{x}\\
&\to -\int_0^T\int_\Omega \bar\rho\,\partial_t\varphi\ \mathrm{d}\boldsymbol{x}\,\mathrm{d}t\ -\int_\Omega\rho_0(\boldsymbol{x})\,\varphi(\boldsymbol{x},0)\ \mathrm{d}\boldsymbol{x}\ \textit{as } m\to+\infty,
\end{aligned}
$$

thanks to the convergence assumption on the approximate solutions and to the convergence of the initial condition for the density (see the corresponding step in this proof). Reordering the summation in $T_2^{(m)}$ *and using* $F_{K,\sigma}^{n+1}=|\sigma|\,\rho_\sigma^{n+1}u_{K,\sigma}^{n+1}$ *yields:*

$$
T_2^{(m)}=-\sum_{n=0}^{N-1}\delta t\sum_{\substack{\sigma\in\mathcal{E}_{\rm int}\\ \sigma=K|L}}|D_\sigma|\ \rho_\sigma^{n+1}\boldsymbol{u}_\sigma^{n+1}\cdot\frac{|\sigma|}{|D_\sigma|}(\varphi_L^n-\varphi_K^n)\,\boldsymbol{n}_{K,\sigma}=-\int_0^T\int_\Omega\rho_{\mathcal{E}}^{(m)}\ \boldsymbol{u}_{\mathcal{E}}^{(m)}\cdot\nabla_{\mathcal{E}}\varphi^{(m)}\ \mathrm{d}\boldsymbol{x}\,\mathrm{d}t,
$$

where $\rho_{\mathcal{E}}^{(m)}$ *and* $\boldsymbol{u}_{\mathcal{E}}^{(m)}$ *are piecewise constant functions on the diamond cells respectively equal to* ρ_σ^{n+1} *(the upwind choice) and* $\boldsymbol{u}_\sigma^{n+1}$ *(average value defined by* (6)*) on each dual cell* D_σ *and time interval* $[t_n,t_{n+1})$*. Thanks to the fact that* $\eta_{\mathcal{M}^{(m)}}\leqslant\eta$ *and to Lemma 4.3, the function* $\rho_{\mathcal{E}}^{(m)}$ *(respectively* $\boldsymbol{u}_{\mathcal{E}}^{(m)}$*) converges to* $\bar\rho$ *(respectively* $\bar{\boldsymbol{u}}$ *) in* $L^r(\Omega)$ *(respectively* $L^r(\Omega)^d$*),* $r\in[1,+\infty)$*; hence, thanks to the weak convergence of the discrete gradient stated in Lemma 4.1, we get*

$$
\lim_{m\to+\infty}-\int_0^T\int_\Omega\rho_{\mathcal{E}}^{(m)}\ \boldsymbol{u}_{\mathcal{E}}^{(m)}\cdot\nabla_{\mathcal{E}}\varphi^{(m)}\ \mathrm{d}\boldsymbol{x}\,\mathrm{d}t=-\int_0^T\int_\Omega\bar\rho\,\bar{\boldsymbol{u}}\cdot\nabla\varphi\ \mathrm{d}\boldsymbol{x}\,\mathrm{d}t.
$$

Momentum balance – Let us then prove that $(\bar\rho,\bar p,\bar{\boldsymbol{u}})$ *satisfies the weak form of the momentum balance equation* (51)*. Let us add the prediction equation* (18) *with the velocity correction equation* (20a)*, and multiply the resulting relation by* $\delta t\ \boldsymbol{\varphi}_K^n$ *and sum for* $n\in[\![0,N-1]\!]$ *and* $K\in\mathcal{M}$*. We obtain* $T_1^{(m)}+T_2^{(m)}+T_3^{(m)}=0$ *with*

$$
\begin{aligned}
T_1^{(m)} &= \sum_{n=0}^{N-1}\sum_{K\in\mathcal{M}}|K|\ \left(\rho_K^n\boldsymbol{u}_K^{n+1}-\rho_K^{n-1}\boldsymbol{u}_K^n\right)\cdot\boldsymbol{\varphi}_K^n,\\
T_2^{(m)} &= \sum_{n=0}^{N-1}\delta t\sum_{K\in\mathcal{M}}|K|\ \ \mathbf{div}_K(\rho^n\boldsymbol{u}^n\otimes\tilde{\boldsymbol{u}}^{n+1})\cdot\boldsymbol{\varphi}_K^n,\\
T_3^{(m)} &= \sum_{n=0}^{N-1}\delta t\sum_{K\in\mathcal{M}}|K|\ \ \boldsymbol{\nabla}_K\,p^{n+1}\cdot\boldsymbol{\varphi}_K^n.
\end{aligned}
$$

With arguments similar to those used for the term $T_1^{(m)}$ *in the mass balance equation, we get*

$$
\lim_{m\to+\infty}T_1^{(m)}=-\int_0^T\int_\Omega\bar\rho\bar{\boldsymbol{u}}\cdot\partial_t\boldsymbol{\varphi}\ \mathrm{d}\boldsymbol{x}\,\mathrm{d}t-\int_\Omega\rho_0(\boldsymbol{x})\,\boldsymbol{u}_0(\boldsymbol{x})\cdot\boldsymbol{\varphi}(\boldsymbol{x},0)\ \mathrm{d}\boldsymbol{x}.
$$

Reordering the summation in $T_2^{(m)}$*, we get, denoting by* $\varphi_{K,i}^n$ *(respectively* $\tilde u_{\sigma,i}^{n+1}$*) the* i*-th com-*

ponent of $\boldsymbol{\varphi}_K^n$ (respectively $\tilde{\boldsymbol{u}}_\sigma^{n+1}$):

$$
\begin{aligned}
T_2^{(m)} &= \sum_{n=0}^{N-1} \delta t \sum_{K\in\mathcal{M}} \sum_{\sigma\in\mathcal{E}(K)} F_{K,\sigma}^n \tilde{\boldsymbol{u}}_\sigma^{n+1}\cdot\boldsymbol{\varphi}_K^n \\
&= \sum_{i=1}^{d}\sum_{n=0}^{N-1} \delta t \sum_{\substack{\sigma\in\mathcal{E}_{\rm int}\\ \sigma=K|L}} |D_\sigma|\ \rho_\sigma^n\ \tilde{u}_{\sigma,i}^{n+1}\ \boldsymbol{u}_\sigma^n\cdot\frac{|\sigma|}{|D_\sigma|}(\varphi_{K,i}^n-\varphi_{L,i}^n)\ \boldsymbol{n}_{K,\sigma} \\
&= -\int_0^T\int_\Omega \rho_{\mathcal{E}}^{(m)}(\boldsymbol{x},t-\delta t^{(m)})\big(\boldsymbol{u}_{\mathcal{E}}^{(m)}(\boldsymbol{x},t-\delta t^{(m)})\otimes\tilde{\boldsymbol{u}}_{\mathcal{E}}^{(m)}\big):\nabla_{\mathcal{E}}\boldsymbol{\varphi}^{(m)}(\boldsymbol{x},t)\ \mathrm{d}\boldsymbol{x}\,\mathrm{d}t
\end{aligned}
$$

where $\rho_{\mathcal{E}}^{(m)}$ and $\boldsymbol{u}_{\mathcal{E}}^{(m)}$ were defined in the mass balance step (and are extended in the previous relation to the time interval $(-\delta t^{(m)},0)$ by the reconstruction of ρ^0 and $\boldsymbol{u}^0$ respectively), and $\widetilde{\boldsymbol{u}}_{\mathcal{E}}^{(m)}$ is defined similarly. Hence, by Lemma 4.3 and Lemma 4.1,

$$
\lim_{m\to+\infty} T_2^{(m)} = -\int_0^T\int_\Omega (\bar\rho\bar{\boldsymbol{u}}\otimes\bar{\boldsymbol{u}}):\nabla\boldsymbol{\varphi}\ \mathrm{d}\boldsymbol{x}\,\mathrm{d}t.
$$

Finally, by Lemma 4.4, we get:

$$
\lim_{m\to+\infty} T_3^{(m)} = -\int_0^T\int_\Omega \bar p\,\mathrm{div}\,\boldsymbol{\varphi}\ \mathrm{d}\boldsymbol{x}\,\mathrm{d}t.
$$

Total energy balance – Let us finally prove that the limit $(\bar\rho,\bar p,\bar{\boldsymbol{u}},\bar e)$ satisfies a weak form of the total energy balance (52). Multiplying the local discrete total energy balance (29) by $\delta t\varphi_K^n$ and summing over the mesh cells and the time steps, we get $T_1^{(m)}+T_2^{(m)}+T_3^{(m)}+T_4^{(m)}+T_5^{(m)}=0$ with

$$
\begin{aligned}
T_1^{(m)} &= \sum_{n=0}^{N-1}\sum_{K\in\mathcal{M}} |K|\ \big((\widetilde{\rho_K E_K})^{n+1}-(\widetilde{\rho_K E_K})^n\big)\ \varphi_K^n,\\
T_2^{(m)} &= \sum_{n=0}^{N-1}\delta t\sum_{K\in\mathcal{M}}\sum_{\sigma\in\mathcal{E}(K)} |\sigma|\ e_\sigma^{n+1}\rho_\sigma^{n+1}u_{K,\sigma}^{n+1}\ \varphi_K^n,\\
T_3^{(m)} &= \sum_{n=0}^{N-1}\delta t\sum_{K\in\mathcal{M}} |K|\ \mathrm{div}_K(p^{n+1}\boldsymbol{u}^{n+1})\ \varphi_K^n,\\
T_4^{(m)} &= \begin{cases}
\dfrac{1}{2}\displaystyle\sum_{n=0}^{N-1}\delta t\sum_{K\in\mathcal{M}}\sum_{\sigma\in\mathcal{E}(K)} |\sigma|\ \tilde{\boldsymbol{u}}_K^{n+1}\cdot\tilde{\boldsymbol{u}}_L^{n+1}\rho_\sigma^n u_{K,\sigma}^n\ \varphi_K^n & \text{if } \delta^{\rm up}=0,\\
\dfrac{1}{2}\displaystyle\sum_{n=0}^{N-1}\delta t\sum_{K\in\mathcal{M}}\sum_{\sigma\in\mathcal{E}(K)} |\sigma|\ |\tilde{\boldsymbol{u}}_\sigma^{n+1}|^2\rho_\sigma^n u_{K,\sigma}^n\ \varphi_K^n & \text{if } \delta^{\rm up}=1,
\end{cases}\\
T_5^{(m)} &= \sum_{n=0}^{N-1}\delta t\sum_{K\in\mathcal{M}} |K|\ P_K^{n+1}\ \varphi_K^n,
\end{aligned}
$$

where $(\widetilde{\rho_K E_K})^n$ is defined by (30). By similar arguments as for the mass and momentum balance equation, we get:

$$
\lim_{m\to\infty} T_1^{(m)} = -\int_0^T\int_\Omega \bar\rho\bar E\ \partial_t\varphi\ \mathrm{d}\boldsymbol{x}\,\mathrm{d}t - \int_\Omega \rho_0(\boldsymbol{x})\,E_0(\boldsymbol{x})\,\varphi(\boldsymbol{x},0)\ \mathrm{d}\boldsymbol{x}.
$$

Reordering the summation in $T_2^{(m)}$ yields:

$$
T_2^{(m)} = \sum_{n=0}^{N-1}\delta t\sum_{\substack{\sigma\in\mathcal{E}_{\rm int}\\ \sigma=K|L}} |\sigma|\ e_\sigma^{n+1}\rho_\sigma^{n+1}\boldsymbol{u}_\sigma^{n+1}\cdot(\varphi_K^n-\varphi_L^n)\,\boldsymbol{n}_{K,\sigma} = -\int_0^T\int_\Omega e_{\mathcal{E}}^{(m)}\rho_{\mathcal{E}}^{(m)}\boldsymbol{u}_{\mathcal{E}}^{(m)}\cdot\nabla_{\mathcal{E}}\varphi^{(m)}\ \mathrm{d}\boldsymbol{x},
$$

where $\rho_{\mathcal{E}}^{(m)}$ and $\boldsymbol{u}_{\mathcal{E}}^{(m)}$ have already been defined and $e_{\mathcal{E}}^{(m)}$ is the piecewise constant function on the dual mesh equal to the upwind choice e_σ on each cell D_σ. Thanks to the assumptions of strong convergence in any L^r, $1 \leqslant r < +\infty$, of the approximate solutions $e^{(m)}$, $\rho^{(m)}$ and $\boldsymbol{u}^{(m)}$ and to the weak convergence of the gradient given by Lemma 4.1, we thus get, invoking Lemma 4.3, that

$$\lim_{m\to+\infty} T_2^{(m)} = -\int_0^T \int_\Omega \bar{e}\bar{\rho}\bar{\boldsymbol{u}} \cdot \nabla\varphi \, \mathrm{d}\boldsymbol{x}.$$

Using the definition (10) *and reordering the summation, we may write the term $T_3^{(m)}$ as*

$$\begin{aligned} T_3^{(m)} &= \sum_{n=0}^{N-1} \delta t \sum_{K\in\mathcal{M}} \sum_{\sigma=K|L} |\sigma| \ (\widetilde{p\boldsymbol{u}})_\sigma^{n+1} \cdot \boldsymbol{n}_{K,\sigma} \ \varphi_K^n \\ &= \sum_{n=0}^{N-1} \delta t \sum_{\substack{\sigma\in\mathcal{E}_{\mathrm{int}} \\ \sigma=K|L}} |D_\sigma| \ (\widetilde{p\boldsymbol{u}})_\sigma^{n+1} \cdot \frac{|\sigma|}{|D_\sigma|}(\varphi_K^n - \varphi_L^n)\, \boldsymbol{n}_{K,\sigma} \\ &= -\int_0^T \int_\Omega (\widetilde{p\boldsymbol{u}})^{(m)} \cdot \nabla_{\mathcal{E}}\varphi^{(m)} \ \mathrm{d}\boldsymbol{x}\,\mathrm{d}t, \end{aligned}$$

where $(\widetilde{p\boldsymbol{u}})^{(m)}$ is the piecewise constant function on the dual mesh defined by:

$$(\widetilde{p\boldsymbol{u}})^{(m)}(\boldsymbol{x},t) = (\widetilde{p\boldsymbol{u}})_\sigma^{n+1} \text{ for } \boldsymbol{x}\in D_\sigma \text{ and } t\in(t_n,t_{n+1}],$$

with $(\widetilde{p\boldsymbol{u}})_\sigma$ defined by (10)*, i.e. $(\widetilde{p\boldsymbol{u}})_\sigma = \alpha_{K,\sigma}\, p_L\, \boldsymbol{u}_K + \alpha_{L,\sigma}\, p_K\, \boldsymbol{u}_L$ for any face $\sigma\in\mathcal{E}_{\mathrm{int}}$, $\sigma = K|L$. Remarking that, since p_L and p_K are positive, the quantity $(\widetilde{p\boldsymbol{u}})_\sigma/(\alpha_{K,\sigma}\, p_L + \alpha_{L,\sigma}\, p_K)$ is a convex combination of $\boldsymbol{u}_K$ and $\boldsymbol{u}_L$, we thus obtain that there exist two reconstruction operators $\mathcal{R}_{1,\mathcal{M}}$ and $\mathcal{R}_{2,\mathcal{M}}$ such that:*

$$T_3^{(m)} = -\int_0^T \int_\Omega \mathcal{R}_{1,\mathcal{M}} p^{(m)} \ \mathcal{R}_{2,\mathcal{M}}\boldsymbol{u}^{(m)} \cdot \nabla_{\mathcal{E}}\varphi^{(m)} \ \mathrm{d}\boldsymbol{x}\,\mathrm{d}t.$$

Thanks to the assumptions of strong convergence in any L^r, $1 \leqslant r < +\infty$ of the approximate solutions $p^{(m)}$ and $\boldsymbol{u}^{(m)}$ and to the weak convergence of the gradient given by Lemma 4.1, we thus get that

$$\lim_{m\to+\infty} T_3^{(m)} = -\int_0^T \int_\Omega \bar{p}\bar{\boldsymbol{u}} \cdot \nabla\varphi \ \mathrm{d}\boldsymbol{x}\,\mathrm{d}t.$$

The convection term, $T_4^{(m)}$, can be rewritten as:

$$T_4^{(m)} = \sum_{n=0}^{N^{(m)}-1} \delta t \sum_{\substack{\sigma\in\mathcal{E}_{\mathrm{int}} \\ \sigma=K|L}} |\sigma| \ \tilde{\boldsymbol{u}}_{\sigma,1}^{n+1} \cdot \tilde{\boldsymbol{u}}_{\sigma,2}^{n+1} \ \rho_\sigma^n \ \boldsymbol{u}_\sigma^n \cdot \left(\frac{|\sigma|}{|D_\sigma|}(\varphi_K^n - \varphi_L^n)\, \boldsymbol{n}_{K,\sigma}\right)$$

where $\tilde{\boldsymbol{u}}_{\sigma,1}^{n+1} = \tilde{\boldsymbol{u}}_K^{n+1}$ and $\tilde{\boldsymbol{u}}_{\sigma,2}^{n+1} = \tilde{\boldsymbol{u}}_L^{n+1}$ in the centered case ($\delta^{\mathrm{up}} = 0$), and $\tilde{\boldsymbol{u}}_{\sigma,1}^{n+1} = \tilde{\boldsymbol{u}}_{\sigma,2}^{n+1} = \boldsymbol{u}_\sigma^{n+1}$ in the upwind case. In both cases, the discrete velocity fields $\widetilde{\boldsymbol{u}}_1$ and $\widetilde{\boldsymbol{u}}_2$ defined by these relations are reconstructions of $\widetilde{\boldsymbol{u}}$. Hence, with the same arguments as for the term $T_2^{(m)}$, we have:

$$\begin{aligned} \lim_{m\to\infty} T_4^{(m)} &= \lim_{m\to\infty} \int_0^T \int_\Omega \widetilde{\boldsymbol{u}}_1^{(m)} \cdot \widetilde{\boldsymbol{u}}_2^{(m)} \rho^{(m)} \widetilde{\boldsymbol{u}}^{(m)} \cdot \nabla_{\mathcal{E}^{(m)}}\varphi^{(m)} \ \mathrm{d}\boldsymbol{x}\,\mathrm{d}t \\ &= \int_0^T \int_\Omega \bar{\boldsymbol{u}}\cdot\bar{\boldsymbol{u}} \ \bar{\rho} \ \bar{\boldsymbol{u}} \cdot \nabla\varphi \ \mathrm{d}\boldsymbol{x}\,\mathrm{d}t. \end{aligned}$$

Finally, the fact that $T_5^{(m)} \to 0$ as $m\to\infty$ is dealt with in Lemma 4.6 below.

Entropy inequality – *Let $\varphi \in C_c^\infty(\Omega \times [0,T), \mathbb{R}_+)$ and let $\varphi^{(m)} = \varphi_{\mathcal{M}^{(m)},\delta t^{(m)}}$ be its interpolate. Multiplying the local discrete entropy inequality* (32) *by $\delta t \varphi_K^n$ and summing over the mesh cells and the time steps, we get $T_1^{(m)} + T_2^{(m)} \leqslant 0$ with*

$$T_1^{(m)} = \sum_{n=0}^{N-1} \sum_{K\in\mathcal{M}} |K|\ (\eta_K^{n+1} - \eta_K^n)\ \varphi_K^n, \quad T_2^{(m)} = \sum_{n=0}^{N-1} \delta t \sum_{K\in\mathcal{M}} \sum_{\sigma\in\mathcal{E}(K)} |\sigma|\ \eta_\sigma^{n+1} u_{K,\sigma}^{n+1}\ \varphi_K^n.$$

Clearly, thanks to the convergence assumtions on $\rho^{(m)}$ and $e^{(m)}$, one has $\eta(\rho^{(m)}, e^{(m)}) \to \eta(\bar\rho, \bar e)$ in L^r for any $r \in [1, +\infty[$, so that by similar arguments as for the mass, momentum and total energy balance equations, we get:

$$\lim_{m\to\infty} T_1^{(m)} = -\int_0^T \int_\Omega \eta(\bar\rho, \bar e)\ \partial_t\varphi\ \mathrm{d}\boldsymbol{x}\,\mathrm{d}t - \int_\Omega \eta(\rho_0, e_0)(\boldsymbol{x})\,\varphi(\boldsymbol{x}, 0)\ \mathrm{d}\boldsymbol{x}.$$

Reordering the summation in $T_2^{(m)}$ yields:

$$T_2^{(m)} = \sum_{n=0}^{N-1} \delta t \sum_{\substack{\sigma\in\mathcal{E}_{\rm int}\\ \sigma=K|L}} |\sigma|\ \eta_\sigma^{n+1} \boldsymbol{u}_\sigma^{n+1} \cdot (\varphi_K^n - \varphi_L^n)\,\boldsymbol{n}_{K,\sigma} = -\int_0^T \int_\Omega \eta(\rho_\mathcal{E}^{(m)}, e_\mathcal{E}^{(m)}) \boldsymbol{u}_\mathcal{E}^{(m)} \cdot \nabla_\mathcal{E}\varphi^{(m)}\ \mathrm{d}\boldsymbol{x}.$$

Again, it is clear that $\eta(\rho_\mathcal{E}^{(m)}, e_\mathcal{E}^{(m)}) \to \eta(\bar\rho, \bar e)$ in L^r for any $r \in [1, +\infty[$, so that by arguments similar as those used for the term $T_2^{(m)}$ in the total energy balance, we get that

$$T_2^{(m)} \to -\int_0^T \int_\Omega \eta(\bar\rho, \bar e)\,\bar{\boldsymbol{u}} \cdot \boldsymbol{\nabla}\varphi\ \mathrm{d}\boldsymbol{x}\,\mathrm{d}t \text{ as } m \to +\infty,$$

which concludes the proof.

Lemma 4.6 (Pressure remainder terms) *Let $(\mathcal{M}^{(m)}, \delta t^{(m)})_{m\in\mathbb{N}}$ be a sequence of meshes and time steps such that $h^{(m)} \to 0$ and $\delta t^{(m)} \to 0$ as $m \to +\infty$, and satisfying* (48)*. Let $(\rho^{(m)})_{m\in\mathbb{N}}$ and $(p^{(m)})_{m\in\mathbb{N}}$ be (part of) the associated sequence of discrete solutions. We assume that the sequences $(\rho^{(m)})_{m\in\mathbb{N}}$ and $(p^{(m)})_{m\in\mathbb{N}}$ satisfy the boundedness assumptions* (44) *and* (45)*. Let $\varphi \in C_c^\infty(\Omega \times [0,T))$, let P_K^{n+1} be given by* (25)*, and let $X^{(m)}$ be defined by*

$$X^{(m)} = \sum_{n=0}^{N^{(m)}-1} \delta t \sum_{K\in\mathcal{M}} |K|\ P_K^{n+1} \varphi_K^n,$$

where φ_K^n is the interpolation of φ defined by (37)*. Then*

$$\lim_{m\to+\infty} X^{(m)} = 0.$$

Proof 9 *The proof of this lemma is similar to the proof of [21, Lemma 3.16], which concerns the same result for the case of a staggered hexaedral or tetrahedral grid and a slightly different discrete gradient. By definition of P_K^n, and thanks to a reordering of the summations, we get*

$$\begin{aligned}
|X^{(m)}| &= \Big| \sum_{n=0}^{N^{(m)}-1} \frac{\delta t^2}{2} \sum_{K\in\mathcal{M}} |K| \Big(\frac{|\nabla_K p^{n+1}|^2}{\rho_K^n} - \frac{|\nabla_K p^n|^2}{\rho_K^{n-1}} \Big)\ \varphi_K^n \Big| \\
&\leqslant \sum_{n=0}^{N^{(m)}-1} \frac{\delta t^2}{2} \sum_{K\in\mathcal{M}} |K| \frac{|\nabla_K p^{n+1}|^2}{\rho_K^n} |\varphi_K^{n+1} - \varphi_K^n| + \frac{\delta t^2}{2} \sum_{K\in\mathcal{M}} |K| \frac{|\nabla_K p^0|^2}{\rho_K^{-1}} |\varphi_K^0|.
\end{aligned}$$

Now, by the definition of the discrete gradient (8)*, and since the coefficients* $\alpha_{K,\sigma}$ *lie in the* $[0,1]$ *interval, we have:*

$$\left|\nabla_K p^{n+1}\right|^2 \leqslant \frac{1}{|K|^2}\left[\sum_{\sigma=K|L}|\sigma|\ |p_L^{n+1}-p_K^{n+1}|\right]\left[\sum_{\sigma=K|L}|\sigma|\ |p_L^{n+1}-p_K^{n+1}|\right]$$
$$\leqslant \frac{1}{|K|^2}\left[\sum_{\sigma=K|L}|\sigma|\ |p_L^{n+1}-p_K^{n+1}|\right]|\partial K|\ \|p\|_\infty.$$

By the definition (47) *of* $\underline{h}_{\mathcal{M}}$*, we have*

$$\frac{|\partial K|}{|K|} \leqslant \frac{1}{\underline{h}_{\mathcal{M}}}.$$

Furthermore, there exists $C_\varphi > 0$ *such that* $\left|\varphi_K^{n+1}-\varphi_K^n\right| \leqslant C_\varphi\ \delta t$ *and* $\|\varphi(.,0)\|_\infty \leqslant C_\varphi$*. Hence,*

$$|X^{(m)}| \leqslant C_\varphi \frac{\delta t^2}{\underline{h}_{\mathcal{M}}}\ \|\frac{1}{\rho}\|_\infty\ \|p\|_\infty\ \left(|p^0|_{BV_x}+|p|_{L^1(BV_x)}\right).$$

Therefore, under assumption (48)*,* $X^{(m)} \to 0$ *as* $m \to +\infty$*.*

5. Numerical results

The numerical results produced by the scheme (17)-(20) use an upwind convection operator in the momentum balance, *i.e.* the parameter δ^{up} is set to 1 in (15). The same tests are also performed with the SLK scheme, as a competing pressure-correction scheme for all-Mach flows, and with the Godunov method as a reference scheme. The SLK scheme is implemented in our numerical code whereas the results from the Godunov method are calculated using the Clawpack 4.3 code, see [3].

First, we consider several 1D Riemann problems to assess the accuracy of the scheme (17)-(20). Then two-dimensional Riemann problems are considered. In both cases an oscillatory behaviour is observed near shocks, which does not affect the L^1 convergence. We show how to cure it with an artificial viscosity method such as in [27].

In all the tests, the non-linear system for the projection-correction step is solved with a simple fixed-point procedure. The sub-iterations are initialised with the most up-to-date flow variables. During a sub-iteration, we successively update the velocity with (20a), solve the density with (20b), update the term S_K^{n+1} with (21), solve the internal energy with (20c) and finally update the pressure with the equation of state. Let n and $k \geqslant 0$ be respectively the time iteration and the fixed-point iteration indices. The stopping criteria for the fixed point sub-iterations is a non-dimensional stagnation criterion defined as:

$$\max\left(\frac{|\boldsymbol{u}^{k+1}-\boldsymbol{u}^k|_\infty}{|\boldsymbol{u}^n|_\infty}, \frac{|\rho^{k+1}-\rho^k|_\infty}{|\rho^n|_\infty}, \frac{|e^{k+1}-e^k|_\infty}{|e^n|_\infty}, \frac{|p^{k+1}-p^k|_\infty}{|p^n|_\infty}\right) < \epsilon$$

The value of ϵ should be chosen so that the mass balance and the internal energy balance are well resolved. A good indicator of whether this is the case is the local residual of the discrete total energy balance (29), since this latter equation is constructed using all the three balance equations. Should any of these balance equations be under-resolved, it would impact the local total energy balance. In our tests, we set $\epsilon = 10^{-6}$, and the residual of the total energy balance is computed at convergence (see Section 5.1.2).

5.1 *Accuracy tests*

5.1.1 *Problem definition* The accuracy of the three schemes is evaluated on seven 1D Riemann problems, with initial states given in Table 1. The domain is $\Omega = [-4,4]$ with Dirichlet boundary conditions on $\partial\Omega$. The solution of the first problem is a pure shock wave (the contact

wave and left shock wave have their amplitude set to zero). Likewise, the solution to the second problem is a pure contact wave, with a left and right non linear wave of zero-amplitude. Riemann problems 3 to 7 are classical problems, see [42]. Test 3 is a Sod shock tube. In Test 4 to Test 7, the genuinely nonlinear waves appearing in the solution are respectively: two rarefaction waves, a left rarefaction wave and a right shock, a left shock and a right rarefaction wave and two strong shocks. The tests are carried out on 6 grids with 2^m cells, $10 \leqslant m \leqslant 15$. The space discretisation step is taken constant to $h = 2^{3-m}$; the time steps δt and total time T are given in Table 1. The convergence orders for the three schemes is summarized in Table 2.

Test	$\rho_{\mathbf{L}}$	$\mathbf{u_L}$	$\mathbf{p_L}$	$\rho_{\mathbf{R}}$	$\mathbf{u_R}$	$\mathbf{p_R}$	**T**	$\delta\mathbf{t}$
1	0.26557	0.92745	0.30313	0.125	0.0	0.1	0.25	$h/1$
2	2.0	2.0	0.4	1.0	2.0	0.4	0.15	$h/2$
3	1.0	0.0	1.0	0.125	0.0	0.1	0.25	$h/1$
4	1.0	-2.0	0.4	1.0	2.0	0.4	0.15	$h/2$
5	1.0	0.0	1000.0	1.0	0.0	0.01	0.012	$h/25$
6	1.0	0.0	0.01	1.0	0.0	100.0	0.035	$h/6$
7	5.99924	19.5975	460.894	5.99242	-6.19633	46.0950	0.035	$h/20$

Table 1. Initial states for the 1D Riemann problems used in accuracy tests.

5.1.2 *Analysis of the results* In Tests 1 to 7, the average number of sub-iterations of the fixed-point procedure is less than 6 for all meshes. The normalized L^∞ residual of the total energy balance is monitored at each timestep t_n:

$$W^n = \frac{\max\limits_{K\in\mathcal{M}} \left| {T_1}_K^n + {T_2}_K^n + {T_3}_K^n + {T_4}_K^n + {T_5}_K^n \right|}{\max\left(\max\limits_{K\in\mathcal{M}} \left|{T_1}_K^n\right|, \max\limits_{K\in\mathcal{M}} \left|{T_2}_K^n\right|, \max\limits_{K\in\mathcal{M}} \left|{T_3}_K^n\right|, \max\limits_{K\in\mathcal{M}} \left|{T_4}_K^n\right|, \max\limits_{K\in\mathcal{M}} \left|{T_5}_K^n\right| \right)}, \text{ with:}$$

$$ {T_1}_K^n = \frac{1}{\delta t}\left((\widetilde{\rho_K E_K})^{n+1} - (\widetilde{\rho_K E_K})^n \right),\ {T_2}_K^n = \mathrm{div}_K(\rho^{n+1} e^{n+1} \boldsymbol{u}^{n+1}), $$

$$ {T_3}_K^n = \frac{1}{2|K|} \sum_{\sigma=K|L} \left|\tilde{\boldsymbol{u}}_\sigma^{n+1}\right|^2 F_{K,\sigma}^n,\ {T_4}_K^n = \widetilde{\mathrm{div}}_K(p^n \boldsymbol{u}^n), \text{ and } {T_5}_K^n = P_K^{n+1}. $$

In each test, the quantity W^n stays below 2×10^{-7} for any timestep n and for any mesh. This confirms the relevance of the stopping criteria chosen for the fixed-point iterations.

Order of convergence – The order of convergence for each test is reported in Table 2. The code using the Godunov solver failed for Test 4 hence the absence of results. The exact solution to the Riemann problems is computed using the method presented in [42]. The L^1 error is calculated as:

$$\mathrm{Err}_{L^1}(w) = \sum_{K\in\mathcal{M}} |K|\ |w_{\mathrm{num},K} - w_{\mathrm{ref},K}|$$

with $w = \{\rho, e, p, u_i\}$, $w_{\mathrm{num},K}$ the numerically computed value and $w_{\mathrm{ref},K}$ the exact reference value.

For a pure shock wave (Problem 1), both the scheme (17)-(20) and the SLK scheme exhibit a convergence order close to 1 for density, pressure and velocity. The two other waves (contact and genuinely nonlinear waves) of the Euler system, whose amplitude is set to zero in the initial data, appear here with a non-zero amplitude. However, this does not seem to impact the convergence order. Let us notice a spurious oscillation at the shock computed with the SLK scheme, which does not occur with the scheme (17)-(20) (see Figure 3).

As to the pure contact wave (Problem 2), both the scheme (17)-(20) and the SLK scheme present an order of convergence close to 0.5 for the density and close to 1 for the pressure and

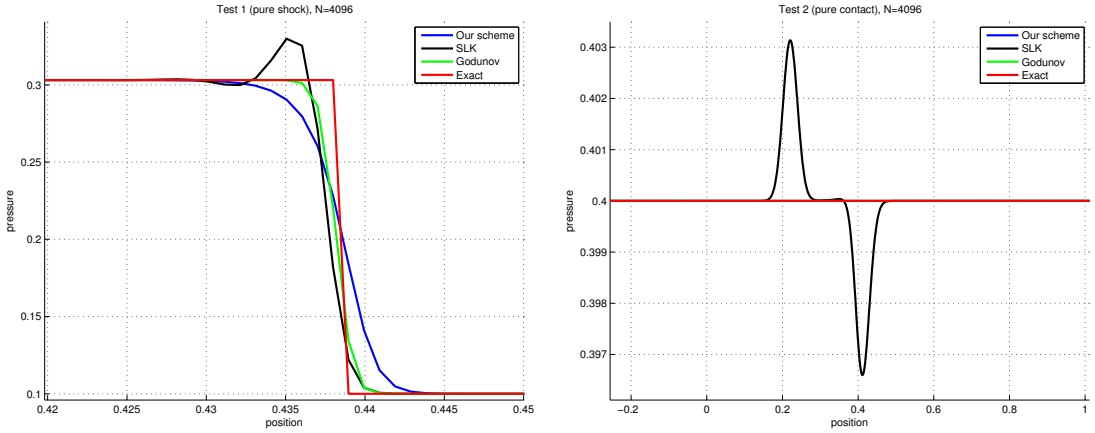

FIG. 3. Final state for Test 1 (left) and Test 2 (right) with the scheme (17)-(20) (blue), the *SLK* scheme (black), the Godunov method (green) and the exact solution (red). The mesh size is $h = 8/4096$.

the velocity. Nonetheless the two schemes differ noticeably: while the SLK scheme presents two waves (shocks) whose amplitude are not zero as they should be, the scheme (17)-(20) preserves the contact wave well and no phantom wave is present in the solution (see Figure 3, right); this agrees with the fact that the scheme was constructed to preserve constant pressure and velocity through a contact discontinuity. For the Godunov method, the order of convergence for non-conserved variables is limited by the order of convergence of the conserved variables on which they depend, hence the lower order of convergence for the velocity and the pressure.

For the Riemann problems 3 to 7, the order of convergence in L^1 norm is between 0.5 and 1. With both schemes, while shocks are sharply captured, contact discontinuities are inaccurately calculated, which is the main source of error in all the tests. The SLK scheme is often slightly more accurate than our scheme even if convergence orders are close. Both schemes suffer from oscillations near shocks. Nevertheless although the magnitude of the oscillations does not decrease with the mesh size, the L^1 measure of these oscillations vanishes; therefore, they do not have a significant impact on the L^1 convergence of error. The issue of the oscillatory behaviour is addressed in the next subsection. Recall that in Test 2, the pressure and velocity are computed exactly by our scheme (precisely speaking, are left to their initial value), as indicated in the table below.

Variable	**Test 1**	**Test 2**	**Test 3**	**Test 4**	**Test 5**	**Test 6**	**Test 7**
ρ (our scheme)	0.989	0.502	0.644	0.658	0.527	0.529	0.544
ρ (SLK)	1.003	0.498	0.634	0.656	0.521	0.517	0.530
ρ (Godunov)	0.975	0.506	0.652	NA	0.563	0.552	0.547
p (our scheme)	0.989	conserved	0.848	0.708	0.877	0.852	1.015
p (SLK)	1.005	1.002	0.818	0.712	0.879	0.855	0.991
p (Godunov)	0.974	0.510	0.797	NA	0.898	0.859	0.933
$\boldsymbol{u}$ (our scheme)	0.982	conserved	0.878	0.679	0.894	0.866	0.994
$\boldsymbol{u}$ (SLK)	0.993	0.924	0.834	0.598	0.891	0.868	0.980
$\boldsymbol{u}$ (Godunov)	0.961	0.506	0.834	NA	0.928	0.875	0.931

Table 2. Convergence orders (L^1 norm) for 1D Riemann problems with our scheme, the SLK scheme and the Godunov method.

Corrective term $\mathbf{S_K^{n+1}}$ – As outlined in the previous sections, the most critical component of our method lies in the corrective term S_K^{n+1} added to the internal energy balance. As

observed in Figure 4, the source term is located at shocks but not at contact discontinuities. Its L^1 measure does not vanish when the space discretisation step tends to zero.

The density field at the final time for Test 7 is given for our scheme with S_K^{n+1} (in blue) and without S_K^{n+1} (in green). The two profiles are similar, however the shock speeds are different, and so are the intermediate states. In absence of the corrective term, the scheme still seems to converge to a limit, but this limit is not a weak solution of the continuous problem (the Rankine-Hugoniot jump conditions are not verified at the shocks).

Let us have a closer look at the behaviour of S_K^{n+1} through its $L^1(0,T;\Omega)$ norm. In the case of an upwind choice in the momentum convection ($\delta^{\rm up}=1$), the correction term reads:

$$S_K^{n+1} = \frac{1}{2\delta t}\rho_K^{n-1}\ \left|\tilde{\boldsymbol{u}}_K^{n+1}-\boldsymbol{u}_K^n\right|^2 + \frac{1}{2|K|}\sum_{\sigma=K|L}|\sigma|\rho_\sigma^n\ (u_{K,\sigma}^n)^-\ \left|\tilde{\boldsymbol{u}}_L^{n+1}-\tilde{\boldsymbol{u}}_K^{n+1}\right|^2,$$

and the L^1-norm of the piecewise constant function S with values S_K^{n+1} reads:

$$\|S\|_{L^1(0,T;\Omega)} = \sum_{n=0}^{N-1}\delta t\sum_{K\in\mathcal{M}}|K|\ S_K^{n+1}. \tag{54}$$

Let us denote by $|(\boldsymbol{u},\tilde{\boldsymbol{u}})|_{L^1(BV_t)}$ the following quantity:

$$|(\boldsymbol{u},\tilde{\boldsymbol{u}})|_{L^1(BV_t)} = \sum_{K\in\mathcal{M}}|K|\sum_{n=0}^{N-1}\left|\tilde{\boldsymbol{u}}_K^{n+1}-\boldsymbol{u}_K^n\right|.$$

Then we easily get:

$$\|S\|_{L^1(0,T;\Omega)} \leqslant \frac{1}{2}\ \|\rho\|_\infty\ \left(\|\boldsymbol{u}\|_\infty+\|\tilde{\boldsymbol{u}}\|_\infty\right)\ |(\boldsymbol{u},\tilde{\boldsymbol{u}})|_{L^1(BV_t)} + \|\rho\|_\infty\ \|\tilde{\boldsymbol{u}}\|_\infty\ |\tilde{\boldsymbol{u}}|_{L^1(BV_x)}.$$

Thus, for a sequence of discretisations, $\|S\|_{L^1(0,T;\Omega)}$ remains bounded provided that the norms and semi-norms at the right-hand side remain bounded. This seems to be true, for the tests performed in the present study. Let us now consider a discontinuity transported at a constant speed over the domain, so that the numerical solution is a travelling profile. Equation (54) yields $\|S\|_{L^1(0,T;\Omega)} = T_1 + T_2$ with:

$$T_1 = \frac{1}{2}\sum_{n=0}^{N-1}\sum_{K\in\mathcal{M}}|K|\ \rho_K^{n-1}\ \left|\tilde{\boldsymbol{u}}_K^{n+1}-\boldsymbol{u}_K^n\right|^2,$$

$$T_2 = \frac{1}{2}\sum_{n=0}^{N-1}\delta t\sum_{K\in\mathcal{M}}\sum_{\sigma=K|L}|\sigma|\rho_\sigma^n\ (u_{K,\sigma}^n)^-\ \left|\tilde{\boldsymbol{u}}_L^{n+1}-\tilde{\boldsymbol{u}}_K^{n+1}\right|^2.$$

The term T_2 equivalently reads:

$$T_2 = \frac{1}{2}\sum_{n=0}^{N-1}\delta t\sum_{\substack{\sigma\in\mathcal{E}_{\rm int}\\ \sigma=K|L}}|\sigma|\rho_\sigma^n\ |u_{K,\sigma}^n|\ \left|\tilde{\boldsymbol{u}}_L^{n+1}-\tilde{\boldsymbol{u}}_K^{n+1}\right|^2.$$

Let us denote $\Delta\tilde{U}$ the amplitude of the discontinuity for the velocity $\tilde{\boldsymbol{u}}$ and $\mathcal{E}_D$ the set of faces inside the numerically computed discontinuity, with $M=\operatorname{card}\mathcal{E}_D$. For $\sigma=K|L\in\mathcal{E}_D$, let ζ_σ^{n+1} be such that:

$$\left|\tilde{\boldsymbol{u}}_L^{n+1}-\tilde{\boldsymbol{u}}_K^{n+1}\right| = \zeta_\sigma^{n+1}\Delta\tilde{U}.$$

If the discontinuity is computed without oscillations, we have $\sum_{\sigma\in\mathcal{E}_D}\zeta_\sigma^{n+1}=1$. With this notation, we get:

$$\sum_{\substack{\sigma\in\mathcal{E}_{\rm int}\\ \sigma=K|L}}|\sigma|\rho_\sigma^n\ |u_{K,\sigma}^n|\ \left|\tilde{\boldsymbol{u}}_L^{n+1}-\tilde{\boldsymbol{u}}_K^{n+1}\right|^2 = \frac{(\Delta\tilde{U})^2}{M}T_D^{n+1},$$

with

$$T_D^{n+1} = M \sum_{\sigma \in \mathcal{E}_D} |\sigma| (\zeta_\sigma^{n+1})^2 \ \rho_\sigma^n \ |u_{K,\sigma}^n|.$$

If the coefficients ζ_σ^{n+1} are all the same, and so equal to $1/M$, T_D^{n+1} is the average of the product $\rho_\sigma^n \ |u_{K,\sigma}^n|$ over the faces involved in the shock. Let us thus consider T_D^{n+1} as a quantity characterising the numerical discontinuity profile, and taking similar values in time. Denoting by T_D the range of T_D^{n+1}, we get:

$$T_2 \simeq \frac{T_D}{2} \ \frac{(\Delta \tilde{U})^2}{M}.$$

Since the discontinuity is supposed to travel trough the mesh at a constant speed, the term T_1 may be estimated with similar arguments. Let us now suppose that the considered discontinuity is a shock, and that the scheme captures the shocks within a number of cells that is independent from the mesh size. This seems to be verified numerically: for instance, with a variation of magnitude greater than 1% of either the left or right state as selection criterion, the left shock is computed within 8 cells and the right shock within 3 cells with all meshes for Test 7. Note that this fact is also consistent with an order one convergence for the tests where the solution is a combination of shock waves. In this case, $\|S\|_{L^1(0,T;\Omega)}$ should remain approximatively constant. On the other hand, if M increases when the mesh is refined (which is the case for contact waves), $\|S\|_{L^1(0,T;\Omega)}$ tends to zero as $h_\mathcal{M}, \delta t \to 0$. Finally, if the velocity is smooth, $\|S\|_{L^1(0,T;\Omega)}$ may be seen to behave as $h_\mathcal{M}$ and δt.

The evolution of S_K^{n+1} in L^1 and L^∞ norm is given in Table 3. Tests 1, 5 and 7 all feature at least one shock wave and the L^1 norm of S_K^{n+1} is kept constant. In contrast, in Test 4 which has two rarefaction waves and one contact wave, the L^1 norm of the compensation term decreases as $O({h_\mathcal{M}}^{0.64})$. As expected, the L^∞ norm of S_K^{n+1} behaves as $O(1/h_\mathcal{M})$ in all tests.

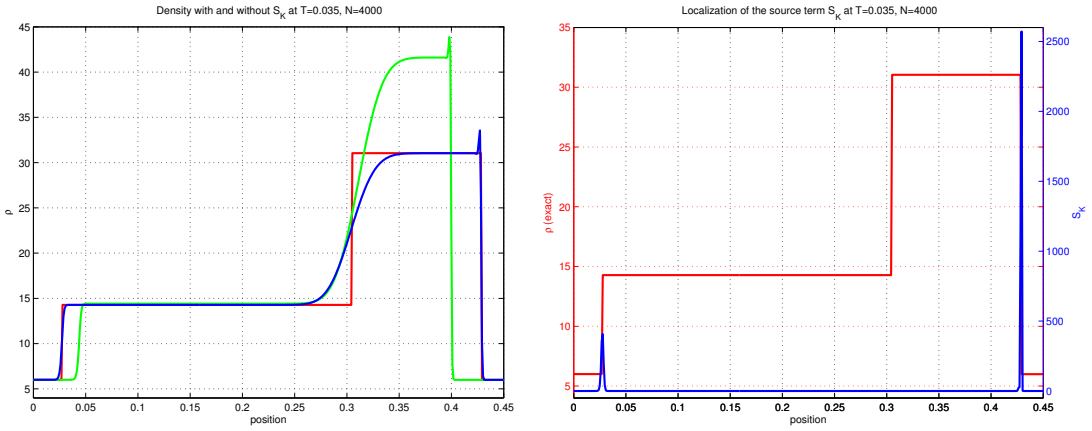

FIG. 4. Influence of the source term for Test 7. Left: density at $T = 0.035$ with S_K (blue), without S_K (green) and exact solution (red). Right: localization of S_K (blue) with respect to the exact solution (red).

5.2 *2D Riemann Problems*

We now test a set of classical 2D Riemann problems, described in detail in [29], for an ideal gas with $\gamma = 1.4$. The computational domain is a square $[0,1] \times [0,1]$ and the initial data consists in four constant states in the quadrants defined by the lines $x = 1/2$ and $y = 1/2$. The 19 initial states are given in figures 5 to 9. According to [29], they represent all the admissible configurations for polytropic gas with only one non-zero-amplitude wave at the 1D Riemann problem between two quadrants, i.e. either a rarefaction (R), shock (S), negative contact (J^-) or positive contact (J^+). On figures 5 to 9 the arrows at the interface between two quadrants indicate a forward or a backward wave. Tests 1 and 2 feature four rarefaction

N	Test 1		Test 4		Test 5		Test 7	
	L^1	L^∞	L^1	L^∞	L^1	L^∞	L^1	L^∞
1024	3.75e-3	8.46e0	4.58e-3	7.72e-1	1.99e1	3.04e5	1.79e2	3.62e6
2048	3.61e-3	1.69e1	3.29e-3	1.54e0	1.97e1	6.08e5	1.78e2	7.23e6
4096	3.55e-3	3.39e1	2.19e-3	3.09e0	1.95e1	1.22e6	1.78e2	1.45e7
8192	3.51e-3	6.77e1	1.39e-3	6.18e0	1.94e1	2.43e6	1.78e2	2.89e7
16384	3.50e-3	1.35e2	8.51e-4	1.24e1	1.93e1	4.86e6	1.78e2	5.79e7
32768	3.49e-3	2.71e2	5.07e-4	2.47e1	1.93e1	9.73e6	1.78e2	1.16e8

Table 3. Evolution of residual term S_K^{n+1} in $L^1(0,T;\Omega)$ and $L^\infty(0,T;\Omega)$ norms.

waves, Tests 3 and 4 four shocks, Tests 5 and 6 four contact waves, Tests 7 to 10 both contact and rarefaction waves, Tests 11 to 14 both contact and shock waves and Tests 15 to 19 contact, shock and rarefaction waves. In all the tests, the problem is discretised with a Cartesian grid with uniform space step $\mathrm{d}x = \mathrm{d}y = 1/400$. The time step is fixed to $\delta t = \mathrm{d}x/10$.

The iso-values of the density calculated with our scheme, the SLK scheme and the Godunov solver for the 19 test cases are given in figures 5 to 9. The wave speeds appear to be correctly calculated by all schemes and the main differences lie in the presence of spurious oscillations. For Test 2, the SLK scheme exhibits oscillations for the rarefaction waves near the bottom left corner of the domain. For Test 3 and 4, both our scheme and SLK suffer from severe oscillations near shocks.

5.3 *Numerical stabilization*

The Weak Local Residual (WLR) method [27] is an interesting and efficient technique for damping spurious oscillations at shock and contact waves by adding an artificial viscosity, controlled by a variable viscosity coefficient μ which is proportional to the weak local residual W of one of the conservation equations. For instance the weak residual of the mass balance reads:

$$W(\phi) = \int_{t=0}^{\infty}\int_{\Omega} \rho\, \partial_t\phi + \int_{t=0}^{\infty}\int_{\Omega} \rho\, \boldsymbol{u}\cdot\boldsymbol{\nabla}\,\phi, \quad \forall \phi \in C^\infty(\Omega\times\mathbb{R}^+).$$

We assume hereafter that the mesh $\mathcal{M}$ is a one dimensional grid with constant step h. The discrete weak local residual is obtained using the piecewise constant approximate solution and the following specific test functions:

$$W_K^{n-\frac{1}{2}} \equiv W(\phi_K^{n-\frac{1}{2}}) = \sum_{n=0}^{\infty}\sum_{P\in\mathcal{M}}\int_{t_n}^{t_{n+1}}\int_P \left(\rho_P^n\partial_t\phi_K^{n-\frac{1}{2}} + \rho_P^n\boldsymbol{u}_P^n\cdot\boldsymbol{\nabla}\,\phi_K^{n-\frac{1}{2}}\right)\,\mathrm{d}\boldsymbol{x}\,\mathrm{d}t$$

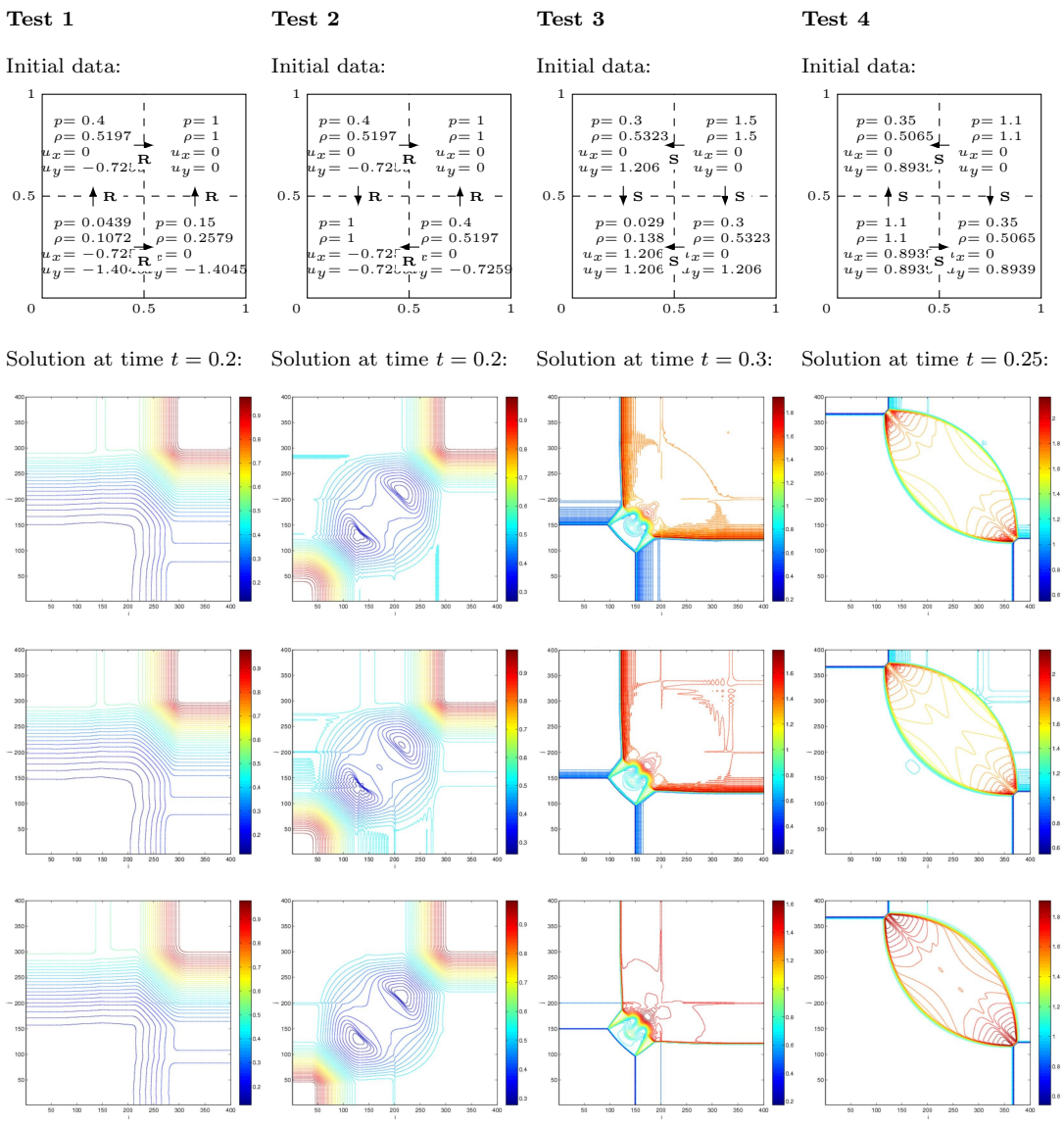

FIG. 5. Density contours (40) for 2D Riemann problems 1 to 4 with our scheme (first row), SLK scheme (second row) and Godunov method (third row).

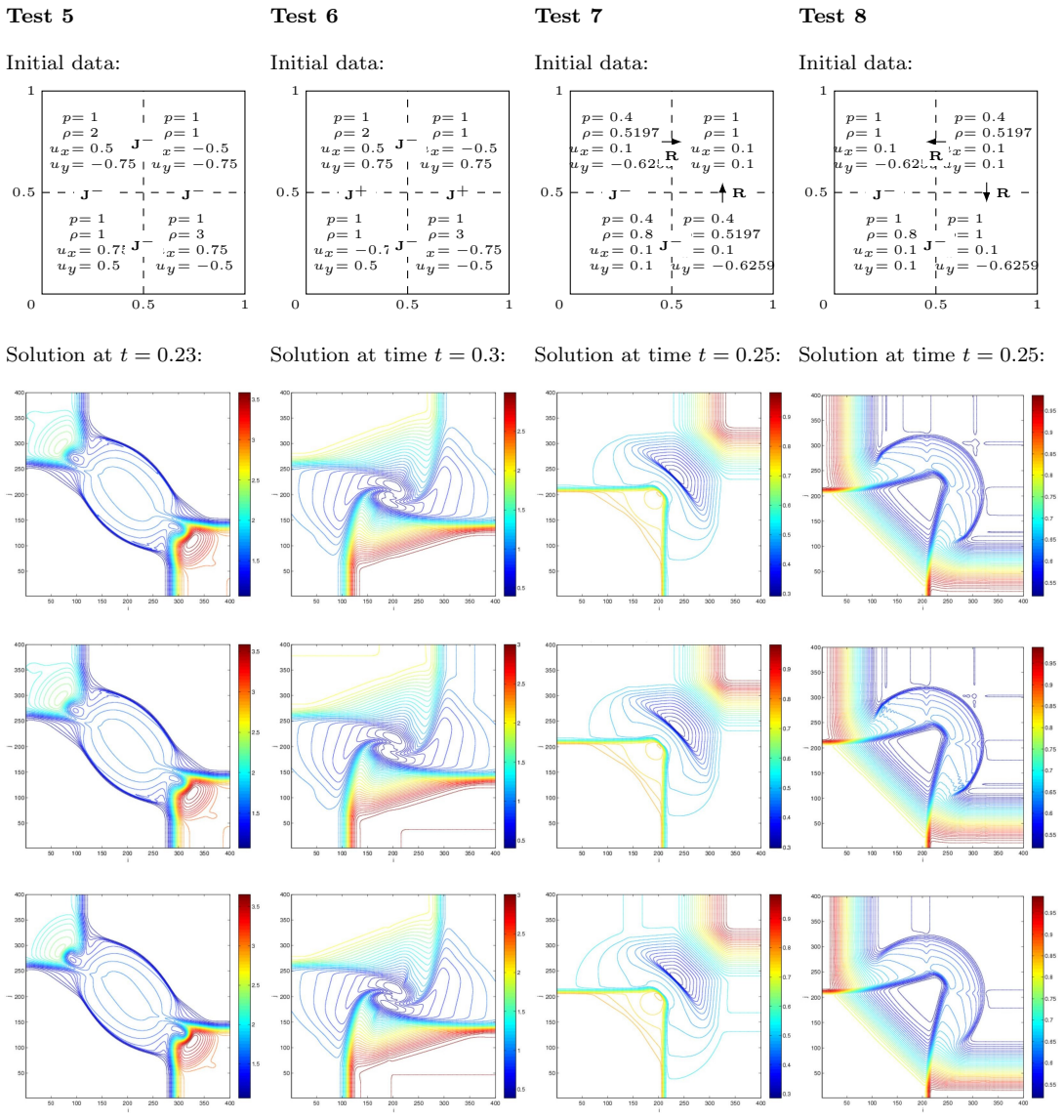

FIG. 6. Density contours (40) for 2D Riemann problems 5 to 8 with our scheme (first row), SLK scheme (second row) and Godunov method (third row).

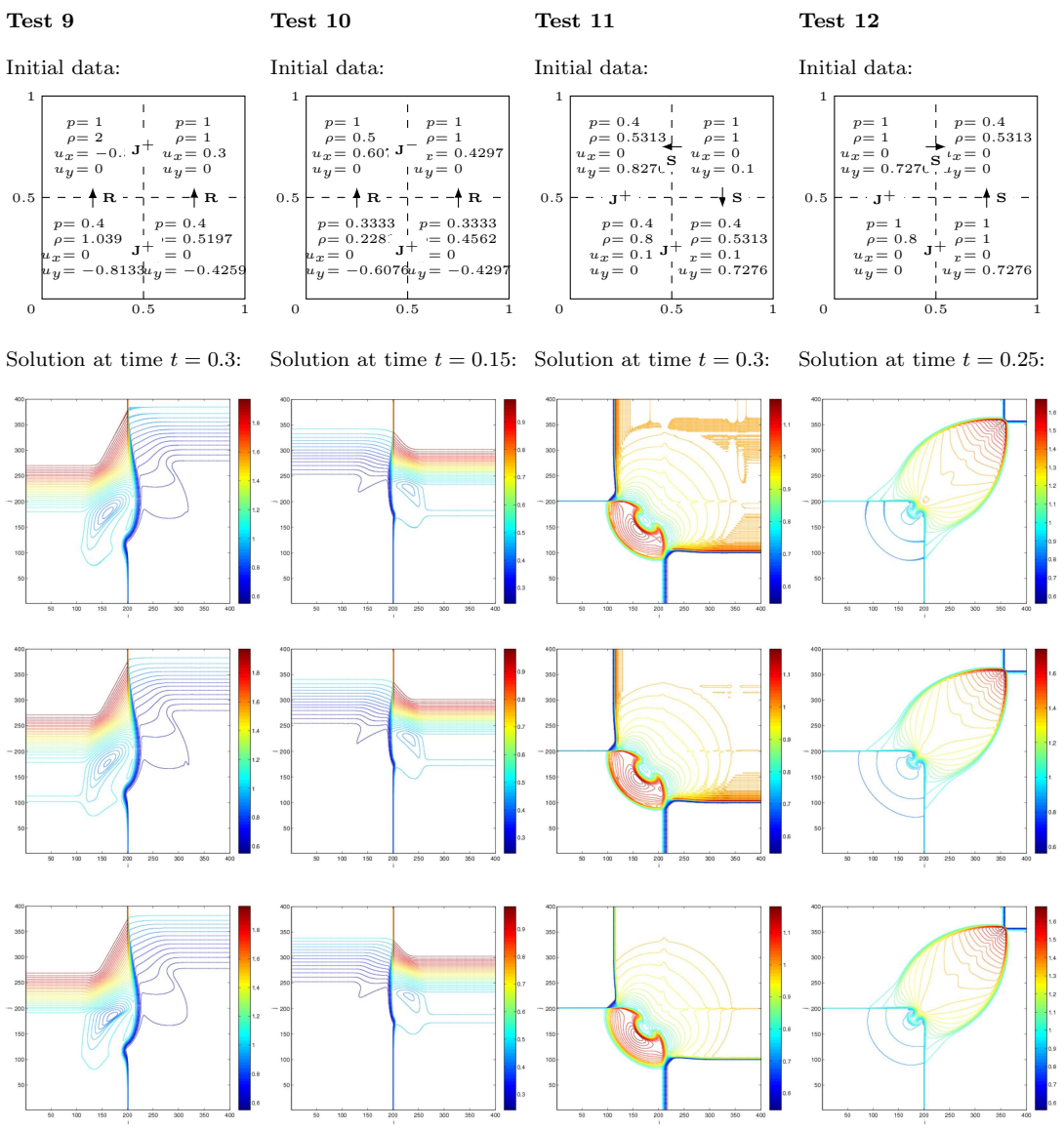

FIG. 7. Density contours (40) for 2D Riemann problems 9 to 12 with our scheme (first row), SLK scheme (second row) and Godunov method (third row).

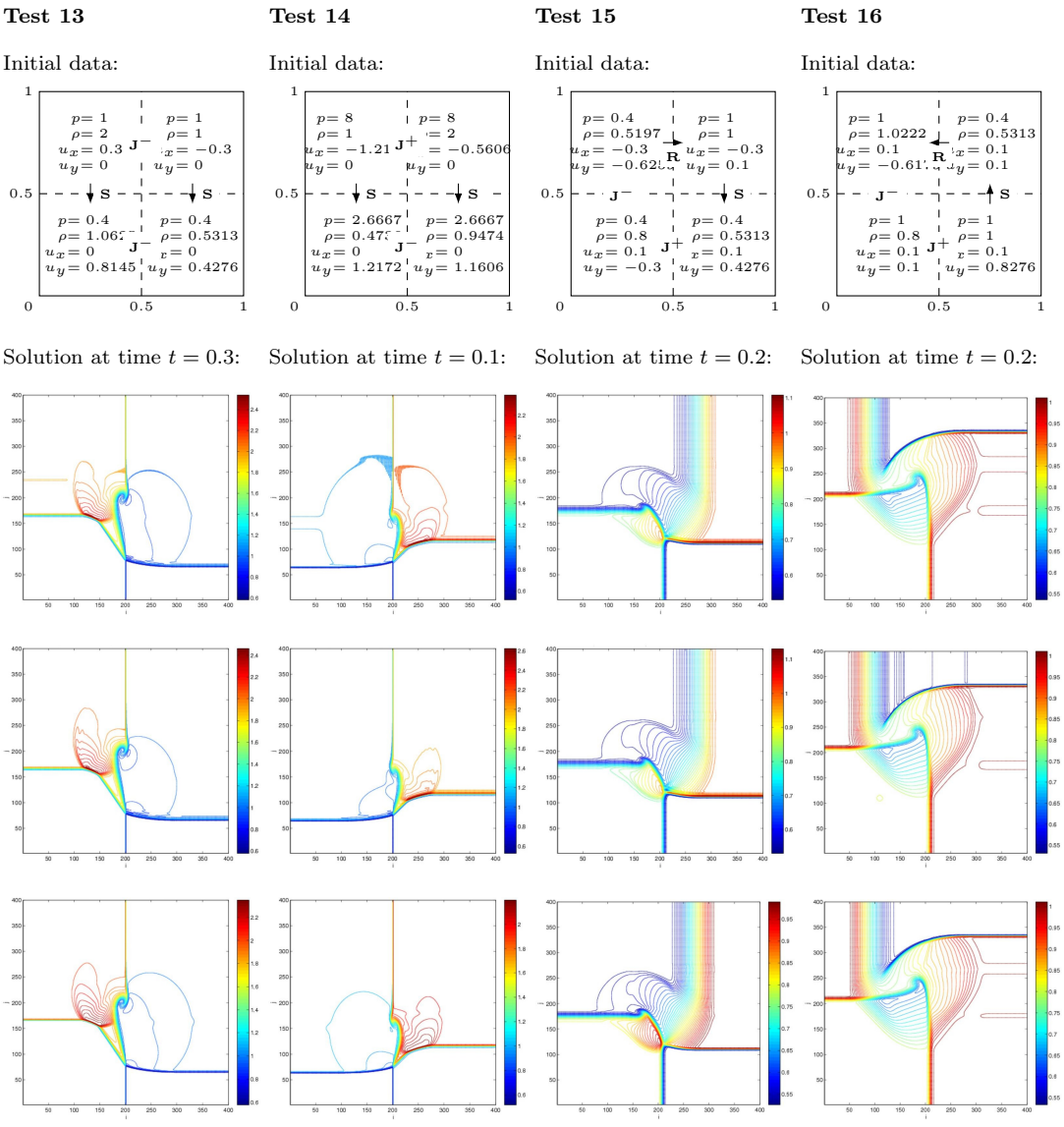

FIG. 8. Density contours (40) for 2D Riemann problems 13 to 16 with our scheme (first row), SLK scheme (second row) and Godunov method (third row).

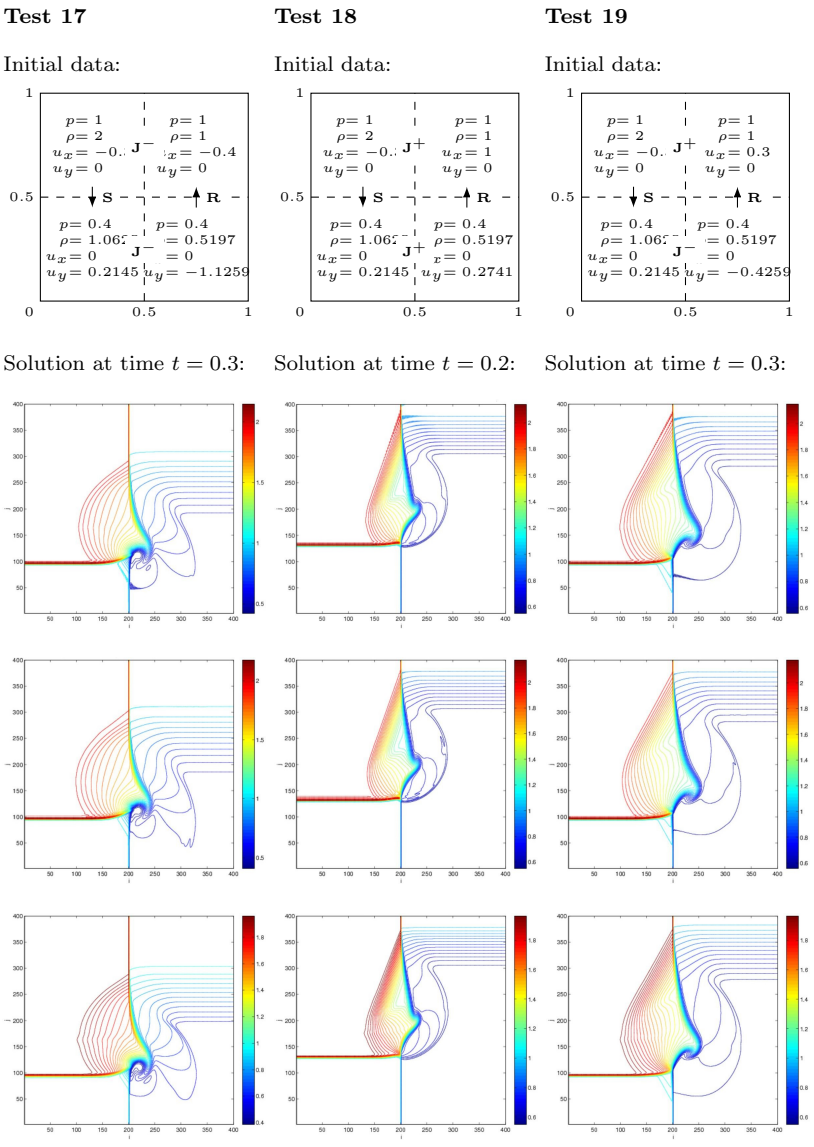

FIG. 9. Density contours (40) for 2D Riemann problems 17 to 19 with our scheme (first row), SLK scheme (second row) and Godunov method (third row).

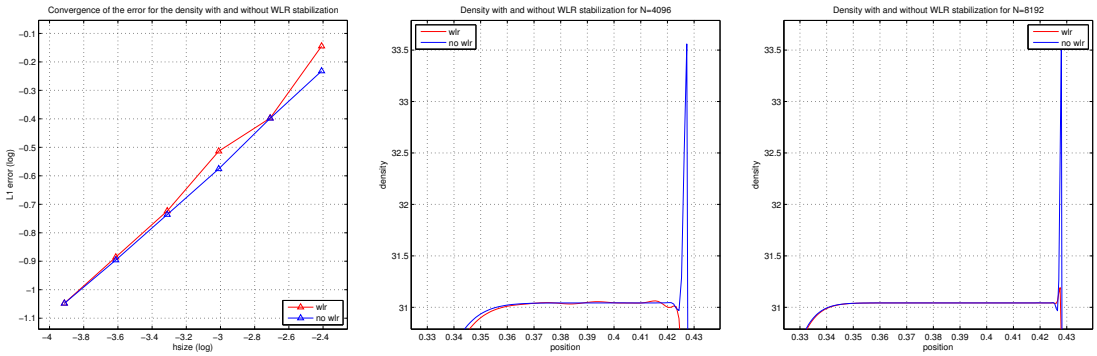

FIG. 10. Application of the WLR artificial viscosity method for our scheme in Test 7: evolution of the error in L^1-norm (left), zoom on the density for $N = 4096$ (center) and for $N = 8192$ (right).

where $\phi_K^{n-\frac{1}{2}}(x,t) = B_K(x) \cdot B^{n-\frac{1}{2}}(t)$ and B_K and $B^{n-\frac{1}{2}}$ are quadratic and linear B-Spline functions:

$$B_K(x) = \begin{cases} \frac{1}{2}\Big(\frac{x-x_K}{h} + \frac{3}{2}\Big)^2 & \text{if } x \in [x_K - \frac{3}{2}h,\ x_K - \frac{1}{2}h) \\ \frac{3}{4} - \Big(\frac{x-x_K}{h}\Big)^2 & \text{if } x \in [x_K - \frac{1}{2}h,\ x_K + \frac{1}{2}h) \\ \frac{1}{2}\Big(\frac{x-x_K}{h} - \frac{3}{2}\Big)^2 & \text{if } x \in [x_K + \frac{1}{2}h,\ x_K + \frac{3}{2}h) \\ 0 & \text{otherwise} \end{cases}$$

$$B^{n-\frac{1}{2}}(t) = \begin{cases} \frac{t - t_n + \frac{3}{2}\delta t}{\delta t} & \text{if } t \in [t_n - \frac{3}{2}\delta t,\ t_n - \frac{1}{2}\delta t) \\ \frac{t_n + \frac{1}{2}\delta t - t}{\delta t} & \text{if } t \in [t_n - \frac{1}{2}\delta t,\ t_n + \frac{1}{2}\delta t) \\ 0 & \text{otherwise} \end{cases}$$

Note that test function $\phi_K^{n-\frac{1}{2}}$ has the local support $3h \times 2\delta t$. The artificial viscosity μ_σ at the face $\sigma = K|L$ is taken proportional to the largest weak local residual among neighboring cells K and L:

$$\mu_{K|L}^n = C_W \max(|W_K^{n-\frac{1}{2}}|, |W_L^{n-\frac{1}{2}}|) \tag{55}$$

The coefficient C_W is tuned by hand as a trade-off between the damping of oscillations and the amount of artificial diffusion introduced. It can be shown that $W_K^{n-\frac{1}{2}}$ is $o(h)$ near shocks, $o(h^\alpha)$ near contact waves with $1 < \alpha \leqslant 2$ and $o(h^3)$ in smooth regions, see [27].

Introducing WLR artificial viscosity with $C_W = 10^2$ in our scheme for Test 7 significantly damps the oscillations (see Figure 10). Despite the added diffusion, the global accuracy of the scheme is not noticeably affected, except for the grid $N = 4096$, in which case the overshoot is indeed completely removed, but the accuracy of the solution is degraded (see Figure 10). The convergence orders in L^1 norm are improved: 0.587 for the density, 1.13 for the pressure and 1.17 for the velocity. However we should note that they are impacted by the poorer accuracy for the $N = 4096$ grid. For other meshes, the accuracy of the solution is the same as the results without WLR and the overshoot, though still present, is severely reduced. For instance the overshoot on the density is reduced by 94% on average.

Let us then turn to the 2D case and focus on Test 3, which seems to be the most impacted

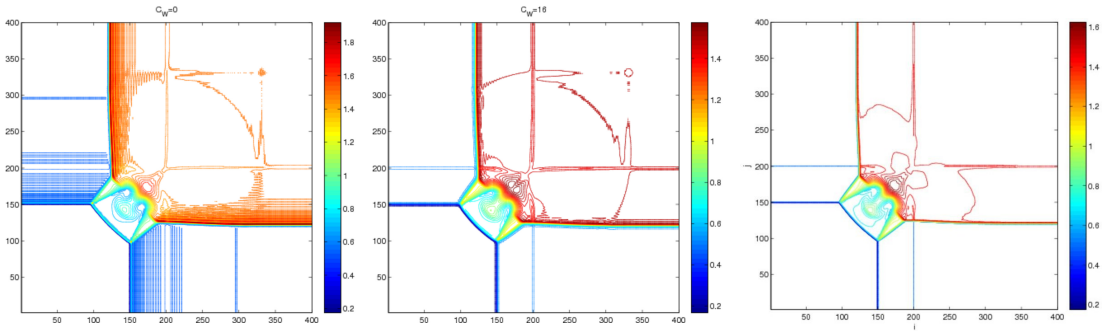

FIG. 11. Density contours (50 values) for 2D Riemann problem 3 computed with our scheme without WLR stabilisation (left), with WLR stabilisation (middle) and the reference solution from the Godunov method (right).

by the spurious oscillations. Similarly to the 1D case, the test function $\phi_K^{n-\frac{1}{2}}$ is defined as:

$$\phi_K^{n-\frac{1}{2}}(x,y,t) = B_K(x) \cdot B_K(y) \cdot B^{n-\frac{1}{2}}(t).$$

The WLR technique is used with a coefficient $C_W = 6.4 \times 10^4$ in (55) (figure 11, right). The oscillations behind shock waves are effectively reduced. Most of the remaining oscillations are in the top-right quadrant $[0, 0.5] \times [0, 0.5]$ and their amplitude is very small. Note however that oscillations remain due to phantom waves; these are shock waves with zero amplitude originating from the initial conditions, see e.g. [10] for examples of such waves.

A. The SLK scheme

The pressure-correction scheme introduced in this paper is compared in Section 5 to the SLK (for "Saturne-LiKe") scheme, introduced in [31] and implemented in the *Code_Saturne* CFD code developed at EDF R&D. Among the differences between our scheme and the SLK scheme, it should be stressed first that the latter is derived from the compressible Euler equations written with the *total energy balance* (1); second, thanks to a decomposition of the variation of the pressure into the variations of the density and of the entropy, the *projection-correction* step of the SLK scheme (here taking the form of an "acoustic step") is linear.

A.1 *Time discretisation*

Among the several variants of the SLK algorithm, we consider the following semi-discrete algorithm from [1]. For all $n \in \mathbb{N}$

Acoustic step (compute $\rho^{n+1}, \boldsymbol{q}^{n+1}$)

$$\frac{\rho^{n+1} - \rho^n}{\delta t} + \operatorname{div} \boldsymbol{q}^{n+1} = 0, \tag{56a}$$

$$\boldsymbol{q}^{n+1} = \rho^n \boldsymbol{u}^n - \delta t (c^2)^n \boldsymbol{\nabla} \rho^{n+1} - \delta t \beta^n \boldsymbol{\nabla} s^n. \tag{56b}$$

Momentum and total energy steps (compute $\boldsymbol{u}^{n+1}, E^{n+1}$)

$$\rho^n \frac{\boldsymbol{u}^{n+1} - \boldsymbol{u}^n}{\delta t} - \boldsymbol{u}^{n+1} \operatorname{div} \boldsymbol{q}^{n+1} + \mathbf{div}(\boldsymbol{u}^{n+1} \otimes \boldsymbol{q}^{n+1}) + \boldsymbol{\nabla} p^n = 0, \tag{57a}$$

$$\rho^n \frac{E^{n+1} - E^n}{\delta t} - E^{n+1} \operatorname{div} \boldsymbol{q}^{n+1} + \operatorname{div} \left[\left(E^{n+1} + \frac{p^n}{\rho^{n+1}} \right) \boldsymbol{q}^{n+1} \right] = 0. \tag{57b}$$

Pressure update (compute p^{n+1})

$$p^{n+1} = (\gamma - 1) \rho^{n+1} \left(E^{n+1} - \frac{1}{2} \boldsymbol{u}^{n+1} \cdot \boldsymbol{u}^{n+1} \right),$$

where $\boldsymbol{q}$ is the "acoustic mass flux" (see [31] for an interpretation of the acoustic step), s the entropy, c the speed of sound and $\beta = \rho^\gamma$.

A.2 *Space discretisation*

We give the space-time discretisation of the SLK scheme for cell-centered finite-volumes that we actually used in the numerical tests:

Initialization

$$\forall K \in \mathcal{M}, \quad \rho_K^0,\ \boldsymbol{u}_K^0,\ p_K^0 \text{ given} \quad ; \quad \rho^{-1} = \rho^0 \quad ; \quad E_K^0 = p_K^0/(\gamma-1)\rho_K^0 - \frac{1}{2}\boldsymbol{u}_K^0 \cdot \boldsymbol{u}_K^0.$$

Iterations for $n = 0, 1, \ldots, N-1$:

1. *Update passive scalar variables*: for all $K \in \mathcal{M}$

$$\begin{aligned} s_K^n &= p_K^n/(\rho_K^n)^\gamma, \\ (c^2)_K^n &= \gamma p_K^n/\rho_K^n. \end{aligned}$$

2. *Predict the density (ρ_K^{n+1})*: solve for all $K \in \mathcal{M}$

$$\begin{aligned} &\frac{|K|}{\delta t}(\rho_K^{n+1} - \rho_K^n) + \sum_{\sigma \in \mathcal{E}(K)} q_{K,\sigma}^{n+1} = 0, \\ &q_{K,\sigma}^{n+1} = |\sigma|\rho_\sigma^n u_{K,\sigma}^n - \delta t|\sigma|(c^2)_\sigma^n(\partial_{K,\sigma}\rho)^{n+1} - \delta t|\sigma|\rho_\sigma^n(\rho_K^n)^{\gamma-1}(\partial_{K,\sigma}s)^n. \end{aligned}$$

3. *Compute the velocity ($\boldsymbol{u}_K^{n+1}$)*: solve for all $K \in \mathcal{M}$

$$\frac{|K|}{\delta t}\rho_K^n(\boldsymbol{u}_K^{n+1} - \boldsymbol{u}_K^n) - \boldsymbol{u}_K^{n+1}\sum_{\sigma \in \mathcal{E}(K)} q_{K,\sigma}^{n+1} + \sum_{\sigma \in \mathcal{E}_(K)} \boldsymbol{u}_\sigma^{n+1} q_{K,\sigma}^{n+1} + \boldsymbol{\nabla}_K\, p^n = 0.$$

4. *Compute the total energy (E_K^{n+1})*: solve for all $K \in \mathcal{M}$

$$\frac{|K|}{\delta t}\rho_K^n(E_K^{n+1} - E_K^n) - E_K^{n+1}\sum_{\sigma \in \mathcal{E}(K)} q_{K,\sigma}^{n+1} + \sum_{\sigma \in \mathcal{E}(K)} \left(E_\sigma^{n+1} + \frac{p_\sigma^n}{\rho_\sigma^{n+1}}\right) q_{K,\sigma}^{n+1} = 0.$$

5. *Update the pressure (p_K^{n+1})*: for all $K \in \mathcal{M}$

$$p_K^{n+1} = (\gamma-1)\rho_K^{n+1}\left(E_K^{n+1} - \frac{1}{2}\boldsymbol{u}_K^{n+1} \cdot \boldsymbol{u}_K^{n+1}\right).$$

The face normal gradient of the entropy and of the density are calculated in the same manner: $\partial_{K,\sigma}s = (s_\sigma - s_K)/d_{K,\sigma}$ with s_σ centred. The pressure p_σ and the advecting velocity $u_{K,\sigma}$ are centred. The face values ρ_σ, $\boldsymbol{u}_\sigma$ and e_σ are calculated with an upwind scheme with respect to the acoustic flux $q_{K,\sigma}^{n+1}$. As to the square of the speed of sound, a harmonic interpolation is used: for a face $\sigma = K|L$,

$$(c^2)_\sigma = \frac{2c_K^2 c_L^2}{c_K^2 + c_L^2}.$$

References

F. Archambeau, J.-M. Hérard, and J. Laviéville. Comparative study of pressure-correction and Godunov-type schemes on unsteady compressible cases. Computers & Fluids, 38:1495–1509, 2009.

A. Chorin. Numerical solution of the Navier-Stokes equations. Mathematics of Computation, 22:745–762, 1968.

Clawpack Development Team. Clawpack software, 2017. Version 5.4.0.

P. Colella and K. Pao. A projection method for low speed flows. Journal of Computational Physics, 149:245–269, 1999.

F. Cordier, P. Degond, and A. Kumbaro. An Asymptotic-Preserving all-speed scheme for the Euler and Navier-Stokes equations. J. Comput. Physics, 231(17):5685–5704, 2012.

K. Deimling. Nonlinear functional analysis. Springer-Verlag, Berlin, 1985.

I. Demirdžić, v. Lilek, and M. Perić. A collocated finite volume method for predicting flows at all speeds. International Journal for Numerical Methods in Fluids, 16:1029–1050, 1993.

R. Eymard and T. Gallouët. H-convergence and numerical schemes for elliptic equations. SIAM Journal on Numerical Analysis, 41(2):539–562, 2000.

R. Eymard, T. Gallouët, and R. Herbin. Finite volume methods. In P. Ciarlet and J. Lions, editors, Handbook of Numerical Analysis, Volume VII, pages 713–1020. North Holland, 2000.

T. Gallouët, J.-M. Hérard, and N. Seguin. A hybrid scheme to compute contact discontinuities in one-dimensional Euler systems. ESAIM: Mathematical Modelling and Numerical Analysis, 36:1133–1159, 2002.

T. Gallouët, R. Herbin, and Latché. On the weak consistency of finite volume schemes for conservation laws on general meshes. Under revision, https://hal.archives-ouvertes.fr/hal-02055794, Mar. 2019.

T. Gallouët, R. Herbin, J.-C. Latché, and K. Mallem. Convergence of the MAC scheme for the incompressible Navier-Stokes equations. Foundations of Computational Mathematics, 18(1):249–289, Feb 2018.

T. Gallouët, R. Herbin, J.-C. Latché, and N. Therme. Entropy estimates for a class of schemes for the Euler equations. Preprint, https://hal.archives-ouvertes.fr/hal-01553699, arXiv:1707.01297, July 2017.

L. Gastaldo, R. Herbin, and J.-C. Latché. A discretization of phase mass balance in fractional step algorithms for the drift-flux model. IMA Journal of Numerical Analysis, 31:116–146, 2011.

D. Grapsas, R. Herbin, W. Kheriji, and J.-C. Latché. An unconditionally stable staggered pressure correction scheme for the compressible Navier-Stokes equations. SMAI Journal of Computational Mathematics, 2:51–97, 2016.

J. Guermond, P. Minev, and J. Shen. An overview of projection methods for incompressible flows. Computer Methods in Applied Mechanics and Engineering, 195:6011–6045, 2006.

F. Harlow and A. Amsden. Numerical calculation of almost incompressible flow. Journal of Computational Physics, 3:80–93, 1968.

F. Harlow and A. Amsden. A numerical fluid dynamics calculation method for all flow speeds. Journal of Computational Physics, 8:197–213, 1971.

F. Harlow and J. Welsh. Numerical calculation of time-dependent viscous incompressible flow of fluid with free surface. Physics of Fluids, 8:2182–2189, 1965.

R. Herbin, W. Kheriji, and J.-C. Latché. Staggered schemes for all speed flows. ESAIM Proceedings, 35:22–150, 2012.

R. Herbin, W. Kheriji, and J.-C. Latché. On some implicit and semi-implicit staggered schemes for the shallow water and Euler equations. ESAIM: Mathematical Modelling and Numerical Analysis, 48(6):1807–1857, 2014.

B. Hjertager. Computer simulation of reactive gas dynamics. Modeling, Identification and Control, 5:211–236, 1985.

Y. Hou and K. Mahesh. A robust, colocated, implicit algorithm for direct numerical simulation of compressible, turbulent flows. Journal of Computational Physics, 205:205–221, 2005.

R. Issa and M. Javareshkian. Pressure-based compressible calculation method utilizing total variation diminishing schemes. AIAA Journal, 36:1652–1657, 1998.

S. Kadioglu, M. Sussman, S. Osher, J. Wright, and M. Kang. A second order primitive preconditioner for solving all speed multi-phase flows. Journal of Computational Physics, 209:477–503, 2005.

M. Kobayashi and J. Pereira. Characteristic-based pressure correction at all speeds. AIAA Journal, 34:272–280, 1996.

A. Kurganov and Y. Liu. New adaptative artificial viscosity method for hyperbolic systems of conservation laws. Journal of Computational Physics, 231:8114–8132, 2012.

J.-C. Latché and K. Saleh. A convergent staggered scheme for variable density incompressible Navier-Stokes equations. Mathematics of Computation, 87:581–632, 2018.

P. Lax and X.-D. Liu. Solution of two-dimensional Riemann problems of gas dynamics by positive schemes. SIAM Journal on Scientific Computing, 19:319–340, 1998.

F.-S. Lien. A pressure-based unstructured grid method for all-speed flows. International Journal for Numerical Methods in Fluids, 33:355–374, 2000.

P. Mathon, F. Archambeau, and J.-M. Hérard. Implantation d'un algorithme compressible dans code_saturne. EDF R&D / MF2E (2004), Technical Report HI-83/03/016/A, 2004.

F. Moukalled and M. Darwish. A high-resolution pressure-based algorithm for fluid flow at all speeds. Journal of Computational Physics, 168:101–133, 2001.

V. Moureau, C. Bérat, and H. Pitsch. An efficient semi-implicit compressible solver for large-eddy simulations. Journal of Computational Physics, 226:1256–1270, 2007.

K. Nerinckx, J. Vierendeels, and E. Dick. Mach-uniformity through the coupled pressure and temperature correction algorithm. Journal of Computational Physics, 206:597–623, 2005.

K. Nerinckx, J. Vierendeels, and E. Dick. A Mach-uniform algorithm: coupled versus segregated approach. Journal of Computational Physics, 224:314–331, 2007.

S. Patankar. Numerical heat transfer and fluid flow. Series in Computational Methods in Mechanics and Thermal Sciences. Washington - New York - London: Hemisphere Publishing Corporation; New York etc.: McGraw-Hill Book Company. XIII, 197 p., 1980.

G. Patnaik, R. Guirguis, J. Boris, and E. Oran. A barely implicit correction for flux-corrected transport. Journal of Computational Physics, 71:1–20, 1987.

E. Politis and K. Giannakoglou. A pressure-based algorithm for high-speed turbomachinery flows. International Journal for Numerical Methods in Fluids, 25:63–80, 1997.

E. Sewall and D. Tafti. A time-accurate variable property algorithm for calculating flows with large temperature variations. Computers & Fluids, 37:51–63, 2008.

R. Temam. Sur l'approximation de la solution des équations de Navier-Stokes par la méthode des pas fractionnaires II. Arch. Rat. Mech. Anal., 33:377–385, 1969.

S. Thakur and J. Wright. A multiblock operator-splitting algorithm for unsteady flows at all speeds in complex geometries. International Journal for Numerical Methods in Fluids, 46:383–413, 2004.

E. Toro. Riemann solvers and numerical methods for fluid dynamics – A practical introduction (third edition). Springer, 2009.

C. Xisto, J. Páscoa, P. Oliveira, and D. Nicolini. A hybrid pressure-density-based algorithm for the Euler equations at all Mach number regimes. International Journal for Numerical Methods in Fluids, online, 70(8):961–976, 2012.